Magn Reson Mater Phy
DOI 10.1007/s10334-017-0631-2

REVIEW ARTICLE

# Towards accurate and precise $T_1$ and extracellular volume mapping in the myocardium: a guide to current pitfalls and their solutions

**Donnie Cameron[1] · Vassilios S. Vassiliou[1,2] · David M. Higgins[3] · Peter D. Gatehouse[2]**

Received: 1 March 2017 / Revised: 5 May 2017 / Accepted: 24 May 2017


**Abstract** Mapping of the longitudinal relaxation time ($T_1$) and extracellular volume (ECV) offers a means of identifying pathological changes in myocardial tissue, including diffuse changes that may be invisible to existing $T_1$-weighted methods. This technique has recently shown strong clinical utility for pathologies such as Anderson-Fabry disease and amyloidosis and has generated clinical interest as a possible means of detecting small changes in diffuse fibrosis; however, scatter in $T_1$ and ECV estimates offers challenges for detecting these changes, and bias limits comparisons between sites and vendors. There are several technical and physiological pitfalls that influence the accuracy (bias) and precision (repeatability) of $T_1$ and ECV mapping methods. The goal of this review is to describe the most significant of these, and detail current solutions, in order to aid scientists and clinicians to maximise the utility of $T_1$ mapping in their clinical or research setting. A detailed summary of technical and physiological factors, issues relating to contrast agents, and specific disease-related issues is provided, along with some considerations on the future directions of the field.

**Keywords** $T_1$ mapping · Accuracy · Precision · Cardiovascular magnetic resonance · Extracellular volume

✉ Donnie Cameron
donnie.cameron@uea.ac.uk

[1] Norwich Medical School, University of East Anglia, Bob Champion Research and Education Building, James Watson Road, Norwich NR4 7UQ, UK

[2] Royal Brompton Hospital and Imperial College London, Sydney Street, London SW3 6NP, UK

[3] Philips Healthcare, Guildford Business Park, Guildford, Surrey GU2 8XG, UK

## Introduction

Mapping of the longitudinal relaxation time, $T_1$, and extracellular volume (ECV) in the human heart has recently shot to prominence on the merits of the modified Look–Locker inversion recovery (MOLLI) imaging sequence and related techniques [1]. These methods allow quantitative tissue characterisation in the myocardium, adding new information to that provided by $T_1$-weighted techniques such as late gadolinium enhancement (LGE) imaging. For focal fibrosis, LGE provides excellent delineation of lesions with some means of quantifying their volume; however, LGE does not give a $T_1$ estimate and may not be able to identify widely distributed or diffuse myocardial diseases. For example, when LGE is applied in diffuse fibrosis, the myocardium can appear isointense and indistinguishable from normal myocardium, as multiple uncalibrated factors affect the image brightness. These are clear limitations of LGE techniques, and in such situations quantitative $T_1$ and ECV mapping is advocated [2, 3]. Use of myocardial $T_1$ mapping is now widespread, with most MRI manufacturers offering $T_1$ mapping solutions. However, great care must be taken when applying these methods clinically, given the need for protocol optimisation and locally-derived normal ranges.

The accuracy and precision of myocardial $T_1$ mapping has been the focus of several studies to date [4–7], and has been discussed to some degree in much of the literature. Innovations in the field are considered in terms of their impact on accuracy and precision, typically offering trade-offs in one or the other for faster or more-accommodating scans. However, there are still several long-standing pitfalls associated with $T_1$ and ECV mapping that affect accuracy and precision, and this review aims to give a comprehensive description of these, along with potential solutions, with the intent of aiding physicists

Published online: 12 June 2017

and clinicians to maximise the clinical utility of $T_1$ mapping. Indications will also be given as to what is reasonably achievable with myocardial $T_1$ mapping in specific clinical applications, without a full clinical review, for which the reader is directed to Haaf et al. [8], Taylor et al. [9], Kammerlander et al. [10], and Schelbert and Messroghli [11], amongst others. The fundamentals of $T_1$ mapping methods, the available pulse sequences, and the history of the technique will be discussed briefly, but again readers are directed to more-detailed reviews for full technical information: for example, by Kellman et al. [5] and Higgins and Moon [12]. Finally, the consensus statement of the Society for Cardiovascular Magnetic Resonance (SCMR) and the CMR Working Group of the European Society of Cardiology can be consulted for recommendations on how to set up a robust $T_1$ mapping protocol [13]. A follow-up parametric mapping consensus statement from the SCMR and the European Association for Cardiovascular Imaging (EACVI) is in preparation.

This review will focus on sources of bias and variability in myocardial $T_1$ and ECV estimation: first, technical and physiological pitfalls; second, issues relating to contrast agents; and third, specific disease-related issues. It will conclude with future directions of the field and some summary recommendations, including guidance on how $T_1$ estimation accuracy might be traded for increased clinical utility. Within each section, pitfalls will be introduced, their mechanisms described, and suggestions offered for how to mitigate or eliminate them, along with possible future solutions, where available. For ease of reference, Table 1 lists the technical and physiological pitfalls discussed in this review in the order they are introduced in the text, with summaries of their relative effects on $T_1$ and ECV mapping accuracy and precision.

## A brief introduction to $T_1$ mapping methodology

All routinely available $T_1$ mapping methods currently rely on preparing the longitudinal magnetisation using inversion or saturation radiofrequency (RF) pulses, applied to the whole imaging volume. Many pulse sequences for $T_1$ mapping can be grouped according to the magnetisation preparation: inversion recovery sequences, including MOLLI [1, 14] and shortened MOLLI (ShMOLLI) [15]; saturation recovery sequences, including independent saturation recovery single-shot acquisitions (SASHA) [16], saturation method using adaptive recovery times for cardiac $T_1$ mapping (SMART$_1$Map) [17], and short acquisition period $T_1$ (SAP-$T_1$) [18]; and mixed preparation sequences, such as saturation pulse-prepared heart-rate independent inversion-recovery (SAPPHIRE) [19]. In practice, a mixture of magnetisation preparations and $T_1$-weighted image acquisitions are performed during a breath-hold, over several cardiac cycles. The aim is to sample the $T_1$ recovery over a range of delay times, and pixel-by-pixel curve-fitting is used to estimate $T_1$ values. This produces a pixelwise $T_1$ map, often with other output maps as quality indicators; see Kellman et al. for a flowchart illustrating the pipeline of $T_1$ and ECV map generation [20]. Most MRI manufacturers provide inline software for map calculation, but open source tools are also available [21, 22].

Non-mapping approaches can also estimate $T_1$ in the heart: the inversion-recovery cine sequence, also known as the Look–Locker cine (LL-cine) technique [23, 24], relies on averaged signal intensities over regions of interest (ROIs) for $T_1$ curve-fitting. This approach uses spoiled gradient recalled echo (GRE) cine, avoiding the factors affecting single-shot balanced steady-state free-precession (bSSFP). Note that many studies that have used the LL-cine method have repeated it at multiple washout times, as this improves ECV accuracy [24].

Given its popularity, the original MOLLI sequence will be considered the default method in this review, with other $T_1$ mapping methods and schemes being addressed where appropriate. A common nomenclature for $T_1$ mapping schemes will also be adopted [5]. This notation lists the number of images acquired following a magnetisation preparation pulse, along with the free-recovery, inter-inversion pause in brackets. Timings are given in beats, "b", or seconds, "s". For example, 3b(3b)3b(3b)5b uses three Look–Locker sets, of three beats, three beats, and five beats, respectively, with pauses of three R–R intervals between each set. A 5s(3s)3s scheme uses two Look–Locker sets and a minimum pause of 3 s between these, rounded up to the next whole R–R interval.

## Technical and physiological sources of error

### Look–Locker correction

The original 3b(3b)3b(3b)5b MOLLI sequence [1] and subsequent optimised versions rely on Look and Locker's correction for rapid $T_1$ estimation: namely, for sampling of the recovering longitudinal magnetisation with a series of small-flip-angle excitation pulses [25, 26]. The magnetisation is perturbed by these excitation pulses, causing flattening of the recovery curve, and yielding an apparent $T_1$, known as $T_1$*, when curve fitting:

$$S(t) = A - B\exp(-TI/T_1^*), \tag{1}$$

where $S(t)$ is the signal at time TI after inversion. The "true" $T_1$ is usually longer than $T_1$* and can be calculated using the so-called Look–Locker correction:

$$T_1 \approx T_1^*(B/A - 1). \tag{2}$$

**Table 1** A summary of technical and physiological pitfalls and their effects on accuracy and precision in $T_1$ and ECV mapping

| Pitfall | Mechanism | Effect on $T_1$ mapping | | Effect on ECV mapping | | Solutions (developing or speculative) |
|---|---|---|---|---|---|---|
| | | Acc. | Prec. | Acc. | Prec. | |
| Look–Locker correction | Assumes continuous, low-flip-angle spoiled GRE; MOLLI $T_1$ mapping can violate these assumptions | •• | • | •• | • | Pauses in seconds, saturation recovery sequence, shallower flip angle |
| Partial volume | Coarse in-plane resolution leads to inclusion of multiple tissues in some voxels, causing $T_1$ errors | •• | •• | •• | •• | Conservative ROI drawing, finer in-plane resolution, (black-blood mapping, slower segmented acquisition) |
| Prep. pulse factors | Adiabatic prep. pulses, robust to $B_0$ and $B_1$ inhomogeneity, are long and lead to $T_2$ decay and $T_1$ bias | ••• | •• | • | • | Appropriate pulse design and/or optimised $B_0$ and $B_1$ shimming |
| Multishot bSSFP readout | Sensitive to $T_2$ and off-resonance and requires catalysation before each imaging readout | ••• | •• | • | • | Appropriate catalysation scheme, coarser in-plane-resolution, shorter TR. Alternatively, use spoiled GRE |
| Field strength | $B_0$ and $B_1$ inhomogeneity ↑ with field strength, $T_1$↑, $T_2$↓, SNR↑ | •• | • | • | • | Appropriate $B_0$ and RF shimming, trading off SNR for shallower flip angle, longer pause intervals |
| *k*-space filling | Linear ordering causes saturation, centric ordering leads to artefacts | • | • | • | • | Linear ordering is adequate, (paired ordering may offer benefits) |
| Signal-to-noise | Noise level affects sampled $T_1$-weighted data when fitting | •• | •• | •• | • | Consider thicker slices, coarser in-plane resolution, using a 3T system |
| Poor breath-holding | Misregistration of source images and $T_1$ error | •• | •• | •• | •• | Patient coaching, image registration, (free-breathing $T_1$ mapping) |
| Cardiac motion | Mistimed acquisitions and misregistration of images | •• | •• | •• | •• | Fit acquisition into diastolic/systolic pause, image registration |
| Flowing blood | Mixture of magnetisation histories in left-ventricular blood | • | • | • | • | Pauses in seconds; position patient carefully or avoid short bore MRI systems, if possible |
| Magnetisation transfer (MT) | Exchange between free and bound water pools distorts $T_1$ recovery, causing $T_1$ underestimation | •• | • | • | • | Lower flip angle, longer TR, saturation recovery sequence. (Alternatively, MT may improve sensitivity to disease) |

This table provides an overview of the pitfalls listed in the text, with no intended significance in the order they appear. The pitfalls are listed with the mechanisms by which they influence $T_1$ and ECV mapping, qualitative ratings of how they affect $T_1$ and ECV accuracy and precision, and possible strategies for eliminating or mitigating them, with developing or speculative solutions shown in brackets. Given the popularity of the original modified Look–Locker inversion recovery (MOLLI) $T_1$ mapping sequence, it is considered the standard here, with other sequences being offered as potential solutions to pitfalls. Ratings are given as one to three blots, with • being mild, •• being moderate, and ••• being severe; however, it should be clear that none of the pitfalls dominate, and their relative importance is highly dependent on the application

*ECV* extracellular volume, *GRE* gradient recalled echo, *RF* radiofrequency, *ROI* region of interest, *SNR* signal-to-noise ratio, *TR* repetition time, and *bSSFP* balanced steady-state free-precession

The Look–Locker correction assumes continual repetition of a small flip angle spoiled GRE readout. MOLLI-based techniques violate the Look–Locker assumptions by using: (1) a bSSFP readout, which is sensitive to $T_2$ and, weakly, to magnetisation transfer (MT), unlike spoiled GRE; (2) a relatively large excitation flip angle, 35° at 1.5T; and (3) an intermittent sampling scheme, governed by heart rate for original MOLLI, to maximise the spread of inversion recovery times. Factors (1) and (2) lead to progressive saturation of the longitudinal magnetisation, causing a negative $T_1$ bias even after Look–Locker correction. Furthermore, Look–Locker sets are separated by pause intervals, aiming to allow sufficient recovery of the magnetisation prior to the next inversion pulse. If any of these pause intervals are too short for the application, be it native or post-contrast, this can lead to additional bias in $T_1$ estimates. This can be particularly problematic for fast heart rates, as well as longer $T_1$ values, such as in native myocardium at 3T.

Bias resulting from limited magnetisation recovery can be mitigated by using an optimised MOLLI acquisition scheme: by extending the inter-inversion pause in beats or by specifying pauses in seconds rather than beats [4]. The 2013 SCMR consensus recommends a 5s(3s)3s scheme for native $T_1$ mapping and a 4s(1s)2s(1s)1s scheme for post-contrast acquisitions [13].

Alternatively, saturation recovery methods such as SASHA [16] sample the recovering longitudinal magnetisation using an independent preparation in each heartbeat, obviating the need for Look–Locker correction over multiple shots at the expense of a loss in precision due to a smaller dynamic range of $T_1$ recovery. The saturation recovery is still affected during each SASHA single-shot readout, but this produces negligible bias in $T_1$ estimates obtained from curve fitting of the independent saturation-recovery images [16, 27].

### Partial volume

Partial volume of different tissues within a voxel is prevalent in $T_1$ mapping with single-shot imaging, where in-plane spatial resolution is necessarily somewhat coarse. Furthermore, the endo- and epi-cardial borders of the myocardium are often oblique to the imaged slice, especially for planes far from the mid-ventricle or in abnormal ventricles. Partial volume can lead to substantial errors, which motivates careful ROI delineation on $T_1$ maps [28].

Partial volume causes bias in the apparent $T_1$, especially when the tissues included in a voxel have strongly different $T_1$ values. Prominent effects occur at the endocardial border where the difference in $T_1$ between blood and myocardium leads to overestimation of native $T_1$ estimation in subendocardial voxels. Partial volume also occurs between myocardium and other tissues, most often fat, whose chemical shift causes variable bias in the pixel $T_1$ [29]; this has clinical relevance, and is discussed further in the "Errors in specific clinical applications" section.

Finer in-plane resolution of the $T_1$ mapping sequence would theoretically reduce partial volume effects, but demands longer single-shot imaging duration if no trade-offs are made, increasing the risk of cardiac-motion blurring. Parallel imaging and partial Fourier in the phase-encode direction are commonly employed to allay this problem. It is essential to avoid partial volume when drawing regions of interest (ROIs), which are often limited to mid-wall when possible [28, 30]. Cardiac motion during the single-shot imaging also corrupts myocardial signal with blood signal in less obvious ways, and is discussed later.

"Black-blood" $T_1$ mapping aims to eliminate blood partial volume for improved $T_1$ estimation accuracy [31], whereby the magnetisation of flowing blood is nulled by motion-sensitive dephasing immediately before each single-shot image. Multiecho fat-water-separated imaging strives to separate fat signal from the thin RV [32], and has been combined with the same method of blood suppression [33]. However, these approaches are not routinely reliable.

To achieve finer spatial resolution, and thus reduce the impact of partial volume in source images on pixelwise mapping, segmented *k*-space image acquisition over multiple cycles is required, and is often combined with some undersampling strategy [34, 35]. Segmented acquisition is severely affected by R–R variability in inversion-recovery methods, and is very slow to acquire the fully recovered image in saturation-recovery methods. The non-mapping LL-cine approach can acquire fine spatial and temporal resolutions, but cardiac motion occurs during recovery, raising questions about the impact of through-slice motion, and substantial post-processing labour is required to optimise ROIs used for curve-fitting and regional estimation of $T_1$.

Finally, free-breathing $T_1$ mapping methods promise to reduce intershot-motion-related errors [36–39]. However, these methods are currently time-consuming.

### Factors affecting magnetisation preparation pulses ($B_1$, $B_0$, $T_2$)

The fitting models used in $T_1$ mapping usually assume exact inversion or saturation of the longitudinal magnetisation, or fit an extra parameter instead, reducing precision. Another approach uses prior knowledge of an inversion factor, which can be estimated from fully relaxed reference images to correct the estimated $T_1$ [40–42].

Conventional RF pulses require accurate RF transmit ($B_1$) fields to achieve their prescribed flip-angle, so are sensitive to $B_1$ inhomogeneity, which can be substantial

across the heart, particularly at 3T [40, 43]. The flip-angle achieved by conventional non-selective RF pulses is also affected by off-resonance errors due to $B_0$ inhomogeneity. Therefore, adiabatic inversion pulses or composite saturation pulses are widely used for mapping to reduce sensitivity to both $B_0$ and $B_1$ inhomogeneity [40, 44]. However, the longer duration of some adiabatic pulses can increase $T_2$ decay during their execution and introduce sensitivity to off-resonance phase accumulation. Kellman, Herzka, and Hansen suggest the use of a relatively short tan/tanh adiabatic pulse for optimal inversion efficiency [40] (Fig. 1), while a composite saturation design is recommended for saturation-recovery methods such as SASHA, provided the higher specific absorption rate and pulse duration are acceptable [44]. Optimised saturation precision, or efficiency, is important in SASHA for two reasons: (1) to enable two-parameter curve-fitting for $T_1$ estimation, as opposed to fitting of saturation efficiency as a third parameter; and (2), reliable removal of any history effect from previous cycles by nulling the longitudinal magnetisation prior to each independent shot.

Although the aforementioned RF pulse designs are more tolerant to $B_0$ and $B_1$ errors, for mapping it is vital to optimise both $B_0$ and $B_1$ over the relevant volume. See Fig. 2 for examples of $B_0$ and $B_1$ maps, in vivo. The advent of RF ($B_1$) shimming hardware with optimised volume calibration methods has enabled substantial improvements in $B_1$ uniformity over the heart [45] even with only two whole-body transmitter channels [46].

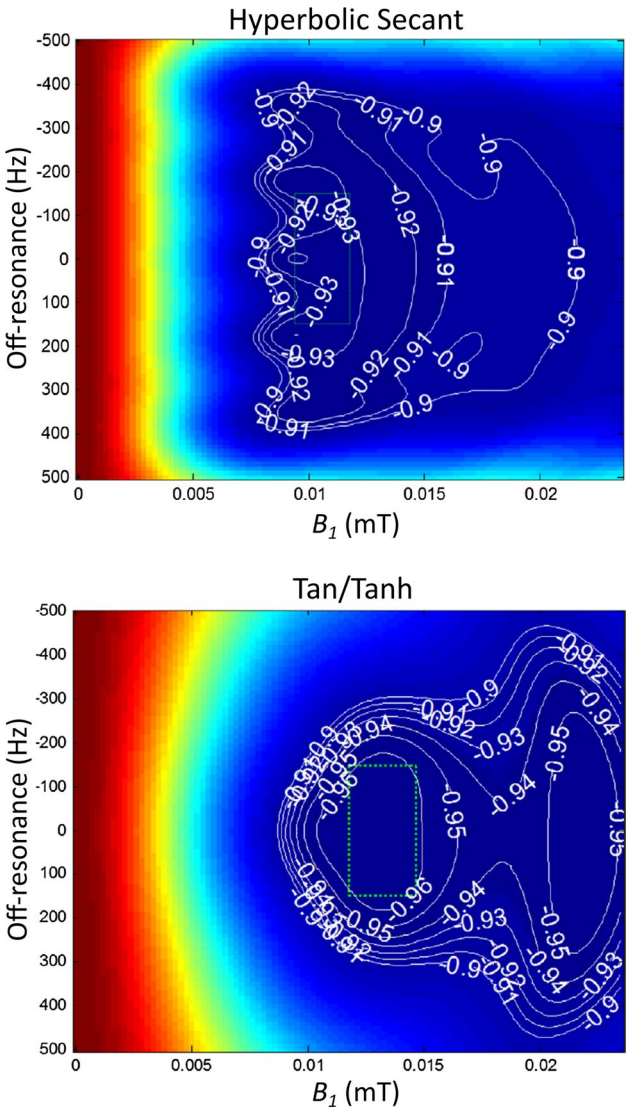


**Fig. 1** Inversion pulse performance. *Plots* show the response to $B_0$ (*vertical*) and $B_1$ (*horizontal*) of two different adiabatic inversion pulse designs: Hyperbolic Secant and Tan/Tanh ($T_1 = 1000$ ms, $T_2 = 45$ ms). A contour value $-1.0$ would indicate perfect inversion. The "design region", enclosing the maximal likely in vivo cardiac $B_0$ and $B_1$ distortion, is represented by the *dotted green box*. Adapted with permission from Kellman et al. [40]

## Inversion-recovery multishot bSSFP

Most $T_1$ mapping methods use bSSFP to sample the recovering longitudinal magnetisation, as this method offers a higher signal-to-noise ratio (SNR) than spoiled GRE. However, bSSFP is sensitive to $T_2$ and off-resonance, where both sensitivities are modulated by excitation flip-angle, RF pulse repetition time (TR), and magnetisation transfer [47]. These factors have greater impact on estimated $T_1$ when the bSSFP flip angle is higher or the TR is longer, and native myocardial $T_1$ values are more affected than the shorter post-contrast $T_1$ values. Off-resonance is larger at 3T, mitigated by use of a lower flip angle [48], but reducing $T_1$ error through use of a shorter TR is largely limited by patient peripheral nerve stimulation [49].

Another consideration with bSSFP is the transient period before the steady-state is established, which is characterised by oscillatory magnetisation, causing image artefacts. The intensity of the oscillations depends on both the bSSFP catalysation used to stabilise the signal, and the *k*-space trajectory [50].

### *Catalysation sequences for bSSFP*

For $T_1$ mapping, some single-shot bSSFP images at short inversion-recovery times are required for optimal curve-fitting, although for SASHA a later start is preferred, as earlier readouts have low SNR [27]. Short delay times prevent stabilisation of the bSSFP signal before phase-encoded data acquisition commences, and since all shots should be acquired with identical parameters, a longer stabilisation for the later inversion-recovery shots is inadvisable.

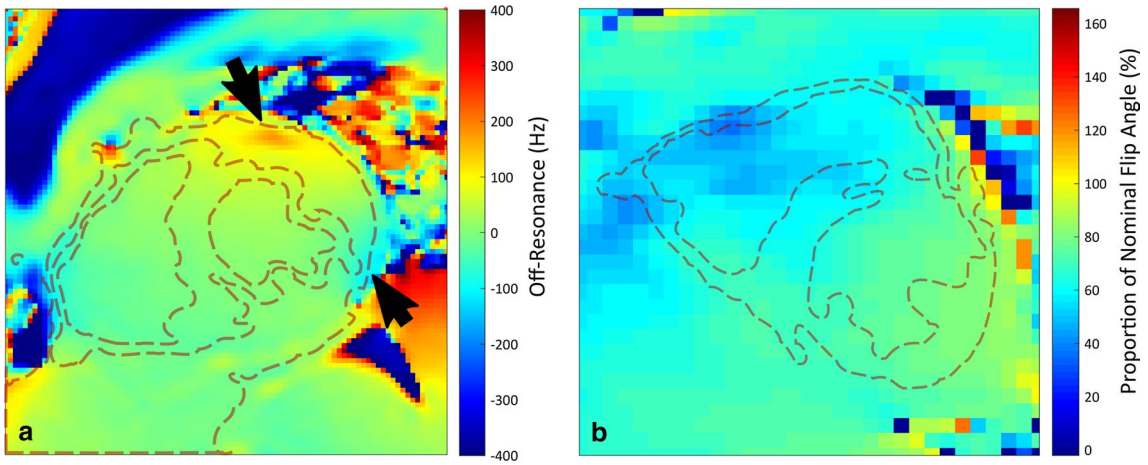


**Fig. 2** In vivo fieldmaps of static field and radiofrequency transmit homogeneity in the heart. *Plots* show a $B_0$ map (**a**) and a $B_1$ map (**b**) planned across the mid-ventricular short axis of the heart, with *dashed red lines* delineating the approximate boundaries of the myocardium. Maps were acquired at 3T, subsequent to first-order $B_0$ shimming and dual-channel RF calibration. Note the distinct inhomogeneity of $B_0$ near the coronary veins in a (*arrows*), and slightly reduced pulse performance across the right ventricle in **b**, where the measured $B_1$ drops to around 50–60% of the nominal value

Several catalysation or "priming" sequences are used in bSSFP to accelerate the signal's approach to the steady state, and these are particularly important in $T_1$ mapping's limited time window before image data must be acquired, especially for centre-out *k*-space ordering, which is discussed later. Catalysation details may be concealed from the scanner's user interface, and may change through software upgrades without warning. Schemes include half-alpha [51], and linear ramp-up [52] (see Fig. 3); the type and duration of the scheme affects $T_1$ estimation accuracy and precision, with bias errors of the order of 5% or more for some approaches [53].

The linear sweep up scheme is a good approach, as this sufficiently quells oscillatory behaviour prior to *k*-space filling [53].

### *Impact of $T_2$ on estimation of $T_1$ by bSSFP readouts*

Shorter $T_2$ relaxation times are associated with underestimation of $T_1$ due to the $T_2/T_1$ weighting of bSSFP [5, 43], and their effect on preparation pulses. The Look–Locker sets of MOLLI sequences are more sensitive to $T_2$ than the independent images used in saturation methods like SASHA, due to accumulated $T_2$-related saturation between single-shot images in each set [54]. When $T_2$ is long, such as in left ventricular blood, MOLLI estimation of $T_1$ increases towards the true value.

In addition to low flip angles and short TR, coarser acquired resolution in tandem with parallel imaging and partial Fourier in the phase-encode direction can reduce the length of the bSSFP pulse train and thus mitigate $T_1$ estimation bias resulting from $T_2$-related saturation.

### *Impact of off-resonance on bSSFP readouts*

A disadvantage of bSSFP is its sensitivity to off-resonance [55], which causes dark banding artefacts and associated $T_1$ errors; however, off-resonance errors in estimated $T_1$ can also occur in myocardial regions without banding artefacts. The inferolateral segment is particularly vulnerable to this problem. Furthermore, the off-resonance sensitivity of bSSFP is also influenced by the catalysation sequence used, as shown in Fig. 3.

The sensitivity to off-resonance is not identical across all of the bSSFP source images. Given that single-shot bSSFP is not fully stabilised for $T_1$ mapping sequences, the impact of off-resonance varies at different points on the $T_1$ recovery curve, and so does not cancel out of the curve-fitting estimation of $T_1$ [48]. ECV measurements are less strongly affected by off-resonance than native $T_1$ estimates, showing a bias error of around 1% or less [48].

Off-resonance errors can be reduced through volume $B_0$ shimming over the heart and great vessels; however, even if second-order $B_0$ shimming is carefully optimised, it cannot correct very local $B_0$ distortions (Fig. 2a). Investigators should familiarise themselves with $B_0$ shimming routines on their scanner, considering factors such as cardiac gating and respiration, among others. Projection-based shimming algorithms [56] are widely available; however, image-based shimming methods [57, 58] may offer better control over local $B_0$, and they provide $B_0$ fieldmaps that can assist quality control of $T_1$ studies.

Off-resonance distortion of $T_1$ can be reduced by lower flip-angles and/or a shorter TR. For example, a coarser frequency-encode resolution may reduce TR; however, this

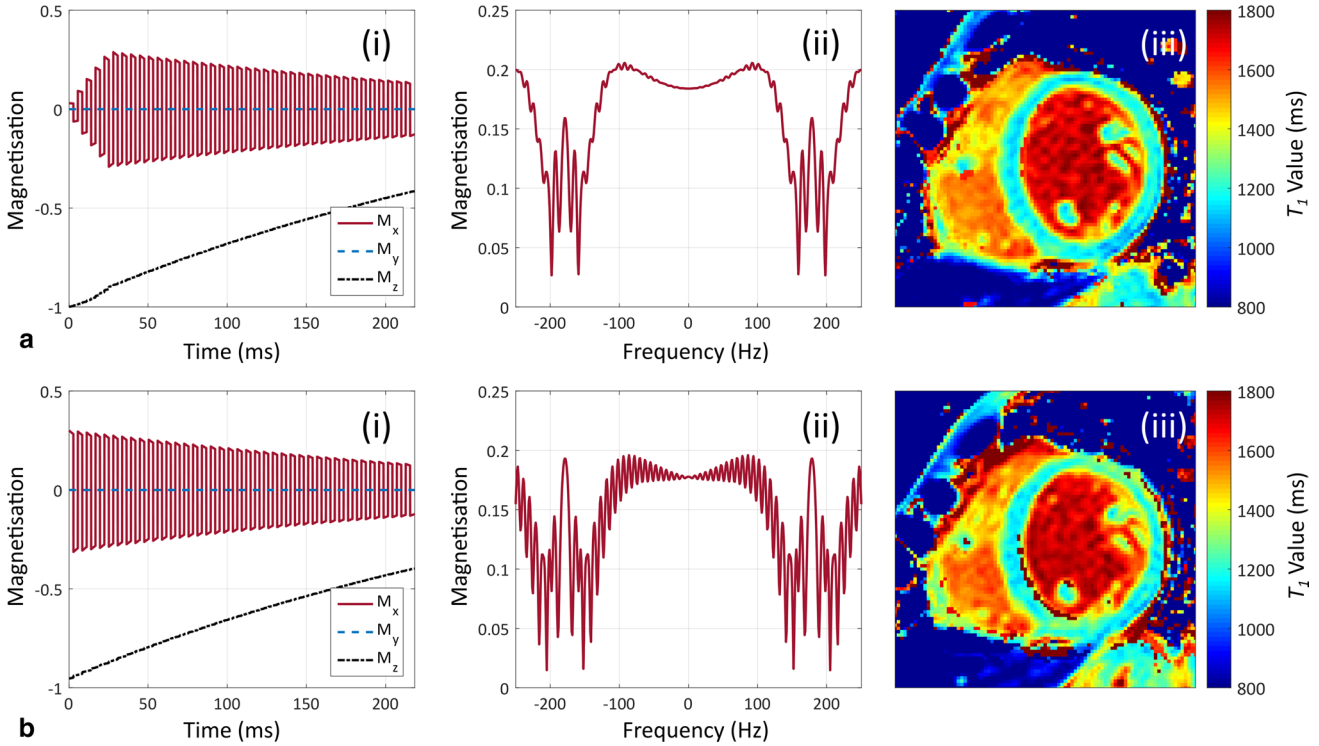


**Fig. 3** The effect of balanced steady-state free-precession catalysation sequences on native $T_1$ maps. *Plots* show the effect of linear ramp-up (**a**) and half-alpha (**b**) catalysations on the magnetisation evolution (*i*) and frequency response at the centre of *k*-space (*ii*) of balanced steady-state free-precession at 3T. Short axis, mid-ventricular native $T_1$ maps are shown for each method (*iii*). Simulations were performed with a repetition time of 2.8 ms, a flip angle of 35°, a $T_1/T_2$ of 1200/45 ms, and 10 catalysation pulses for each method, with a further 39 pulses before the centre of *k*-space

may also automatically modify the phase-encode resolution, reducing the number of RF pulses before the centre of *k*-space and affecting stabilisation. Furthermore, coarser frequency-encode spatial resolution increases partial volume. Any such changes require attention with regards to effects on estimated $T_1$ and possible invalidation of normal range data [13].

A recent development substituted MOLLI's bSSFP readout with a spoiled GRE sequence [59], which avoids the more complex sensitivities of bSSFP, improves $T_1$ estimation accuracy, and reduces the sensitivity of $T_1$ estimation to $T_2$. It has also been applied in patients with implanted devices that cause severe off-resonance artefacts, precluding bSSFP imaging [60]. However, these benefits come with several disadvantages: spoiled GRE shows reduced SNR versus bSSFP; its $T_1$ estimation precision is also reduced; and adequate spoiling may be difficult. Spoiling has been shown to be problematic for the variable flip angle method [61], but may be less so for inversion-recovery based $T_1$ mapping [59].

## Schemes for *k*-space filling

To date, most $T_1$ mapping has used linear phase-encode ordering, where phase-encoding gradient amplitudes are stepped through incrementally. This avoids eddy-current-related signal perturbations, but causes progressive $T_2$-related saturation in the approach to the centre of *k*-space, leading to $T_1$ underestimation. Alternatively, centric phase-encode ordering, also known as the centre-out or low–high approach, fills *k*-space from the centre outwards with alternating and increasing phase-encoding gradient amplitudes; this avoids the $T_2$-related saturation of linear ordering at the expense of increased eddy-current-related artefacts [53].

Although linear-ordering is typically used, several other phase-encode ordering schemes have been investigated to date [43, 53, 62]. Paired phase-encoding has been proposed to mitigate the artefacts associated with centric ordering [63]; however, it has shown mixed results for $T_1$ mapping [53, 62], performing well only with longer catalysation schemes.

## Signal-to-noise

All $T_1$ mapping methods acquire multiple $T_1$-weighted source images, each of which has its own SNR per tissue, and the noise level will influence the sampled points during curve-fitting. The fewer $T_1$-weighted source images used to reconstruct a $T_1$ map, the poorer the curve-fit conditioning

and the poorer the $T_1$ estimation precision [15]. Given the limited number of shots taken throughout longitudinal recovery, their optimum distribution in comparison to the relevant range of $T_1$ is also important, motivating different sequence schemes for native and for post-contrast mapping [5, 27].

SNR varies spatially across the heart, predominantly due to the sensitivity profile of the receiver coil array. Low SNR is most evident in the lateral wall, which is farthest from the coil, and thus this region is more prone to noise-related $T_1$ estimation bias and dispersion [4]. This effect is in addition to susceptibility artefact seen in the lateral wall—another reason why clinical $T_1$ measurements for assessment of diffuse fibrosis are often confined to the interventricular septum [30].

Imaging at higher field strengths can mitigate errors resulting from low SNR, as shown by Piechnik et al. [15], who reported approximately 30% reduction in coefficients of variation for MOLLI and ShMOLLI $T_1$ estimates when moving from 1.5 to 3T. Conversely, 3T exacerbates off-resonance and $B_1$ inhomogeneity effects, though their impact can be controlled.

### Influence of field strength

In addition to the aforementioned off-resonance and $B_1$ inhomogeneity issues at higher field strengths, and the potentially increased SNR, there are also differences in native $T_1$ and $T_2$ values between 1.5 and 3T.

A large multicentre study of native $T_1$ and ECV values in normal myocardium, using original 3b(3b)3b(3b)5b MOLLI, reported mean (standard deviation) native $T_1$ values of 950 (21) ms at 1.5T and 1052 (23) ms at 3T, and mean (standard deviation) ECVs of 0.25 (0.04) at 1.5T and 0.26 (0.04) at 3T [64]. The increased $T_1$ at 3T can lead to insufficient longitudinal recovery between Look–Locker sets, causing $T_1$ underestimation; furthermore, reduced myocardial $T_2$ at 3T relative to 1.5T introduces additional negative bias due to the $T_2/T_1$ weighting of bSSFP and signal decay during preparation pulses [5].

Increased $B_0$ and $B_1$ inhomogeneity at 3T can be mitigated using appropriate $B_0$ and RF shimming, respectively. Shallower excitation flip angles can also allay these effects, if the increased SNR at 3T is traded off [5].

### Breath-holding

Currently, $T_1$ mapping requires breath-holding to minimise respiratory motion while source images are acquired. Original MOLLI used a breath-hold duration of approximately 17 cardiac cycles [1], while newer variants require around 10 or 11 s [4]. A shorter breath-hold is an advantage in routine work [15], but it causes a reduction in SNR. Imperfect breath-holds typically lead to misregistered source images, which corrupt the set of signal intensities used for pixel-by-pixel curve fitting and, in turn, decrease $T_1$ estimation accuracy and precision. Often, misregistration is not readily apparent in calculated $T_1$ maps, unless a confidence-map is provided alongside or overlaid on the $T_1$ map. See Fig. 4 for an example of this.

Post-acquisition quality control has some aspects in common for respiratory motion and cardiac misgating or arrhythmia: $T_1$ mapping source images should be examined carefully for displacements, even if motion-corrected images are also available. Mislocated tissue in or through the selected slice, for any of the shots, may preclude correct mapping of localised disease, such as myocarditis. If significant displacements are found, nonrigid registration may register most myocardial pixels [20, 65], but cannot correct through-slice displacement. Input image registration in $T_1$ mapping is challenging due to the large image-contrast variations between source images, and can be unreliable when tissues are imaged near the null point of longitudinal magnetisation recovery. While there are strategies for dealing

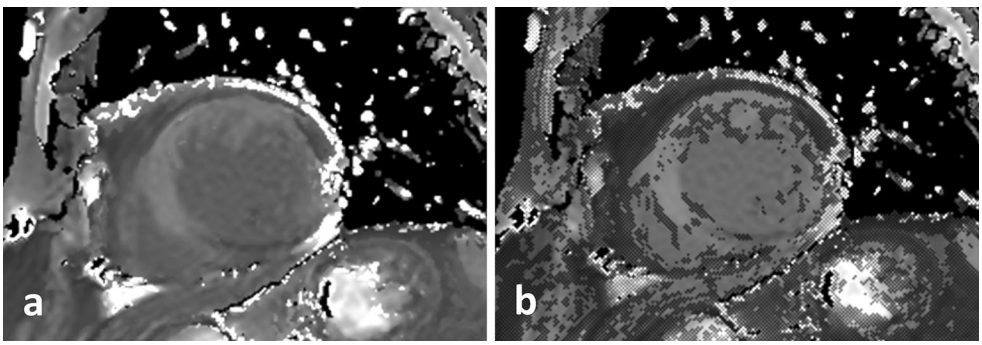


**Fig. 4** An example of motion-related $T_1$ estimation error shown on quality control maps. A short-axis native $T_1$ map corrupted by respiratory motion (**a**) demonstrates excessive pixelwise curve-fitting residual errors, indicated on a confidence map (**b**) by the addition of marked pixels to the same map shown in **a**

with this issue [65], motion-corrected images should be reviewed before drawing ROIs on the $T_1$ map. This issue is another reason why midwall, septum-only ROIs tend to be more reliable.

Free-breathing $T_1$ mapping acquisitions have been reported [34, 36–39], and aim to automatically exclude images with large misregistrations. While this may be more feasible for independent images, as used in SASHA [16], the impact of poor breath-holding or misgating variations on the later points of a Look–Locker set is convoluted. Furthermore, these methods can extend scan time, and often employ undersampling.

### Cardiac triggering and cardiac motion

Source images for mapping must be acquired in the same phase of the cardiac cycle to ensure registration for pixel-wise $T_1$ map calculation.

Some variation in R–R interval is normal, and MOLLI-variant sequences record the real-time R–R increments to the inversion-recovery time during each Look–Locker set. Arrhythmia may be tolerable provided the trigger to the pulse sequence is followed by a reasonably normal ventricular contraction and diastolic pause (diastasis). If arrhythmia interferes with diastolic timing, it is feasible to acquire the single-shot images in end-systole [66, 67]. The end-systolic duration is less dependent on heart rate than diastasis, and may offer improved accuracy and precision in arrhythmia. Partial volume may also be less of an issue, as the contracted myocardium is thickened; however, the brevity of the end-systolic pause necessitates a shorter single-shot image readout, and thus spatial resolution is coarser.

A slightly shorter native $T_1$ has been reported for mapping at end systole versus end diastole [66, 67]; however, this relationship flips after contrast administration, impacting ECV [68]. The cardiac phase of the image does not imply that the entire, usually slower, $T_1$-relaxation process is sensitive to the myocardial relaxation or contraction state at the time of the image.

Similar to respiratory motion, cardiac mistriggering causes mis-registration of source images for $T_1$ mapping. Again, an elastic image registration algorithm may be able to account for this, but source images should be checked rigorously. If mis-registration goes uncorrected, distortion of fitted $T_1$ recovery curves is likely, particularly in the subendocardium. For this reason, some types of cardiac arrhythmia can be a major problem, but novel methods promise robust performance in such conditions [69].

The single-shot imaging duration should not exceed the length of the cardiac pause, be it diastolic or systolic. Tong et al. empirically estimated that the shot duration should not exceed 150 ms for minimal cardiac motion artefacts [70]. It is relatively straightforward to plan single-shot imaging to coincide with the required cardiac phase, as timings can be measured from a bSSFP cine acquired during routine setup, or may be semi-automated [71].

The image-readout duration can also be reduced using parallel imaging methods that acquire coil profiles separately: namely, before the scan or immediately after the last single-shot image. Note a related pitfall with coil profiles or any other prescan applied immediately prior to a $T_1$ mapping acquisition is that the longitudinal magnetisation may not have recovered before the first inversion [48], though this is usually avoided with a pause for breath hold instruction to the patient.

### Flowing blood

Measurement of blood $T_1$ is important for the calculation of ECV. Complications in Look–Locker correction arise for blood that is at least partially replaced by fresh wash-in in the image slice for each cardiac cycle. Completely "fresh" blood, while still acted upon by the initial non-selective inversion, has not experienced previous shots of the current Look–Locker set since inversion and, therefore, does not require Look–Locker correction. However, even a normal heart ejects only around 55–75% of left ventricular blood per cycle [72], so the true situation is probably a complex mixture of different magnetisation histories in left-ventricular blood. Furthermore, in the extreme case, for later images of a native $T_1$ mapping acquisition the arriving blood may have experienced a distorted magnetisation preparation at some upstream location, despite application of optimised preparation pulses. This can occur in short bore scanner systems [5], or in unusual flow pathways following repairs of congenital heart defects.

### Magnetisation transfer (MT)

When estimating $T_1$ in the myocardium and blood pool, it is also important to consider the MT phenomenon, which has been shown to influence the accuracy of $T_1$ mapping [5, 47]. Exchange between free and bound water pools within the tissue of interest reduces the bSSFP signal [73]. For inversion-recovery-based $T_1$ mapping, the bound pool is mostly unaffected by the inversion pulse, so exchange during the long inversion-recovery delays distorts the shape of the $T_1$ recovery curve and introduces $T_1$ underestimation. The extent of this effect varies between tissues, and is substantially smaller in blood than in myocardium [5, 74].

The MT effect can be allayed by using SASHA with a three-parameter curve-fit, at the expense of reduced $T_1$ estimation precision. It can also be mitigated in inversion-recovery $T_1$ mapping by use of lower-flip-angle excitation pulses and a longer imaging TR. Alternatively, the MT effect could be exploited in native $T_1$ mapping for greater

disease discrimination in pathologies such as myocardial infarction (MI), ischaemia, and iron overload—all of which have all demonstrated MT.

### Summary of technical pitfalls

Each technical and physiological challenge listed here may cause errors in $T_1$ and ECV mapping, increasing bias, scatter, or both. Cardiac and respiratory motion are particularly problematic, and strict quality control routines may help correct these where possible. At 3T, inhomogeneous $B_0$ and RF transmit fields also become prominent sources of error, which may be mitigated with appropriate $B_0$ shimming and RF transmit calibration. However, despite these prominent pitfalls, no issue dominates, and with considerable expertise, care, and attention to multiple factors, users can mitigate many sources of error, with the level of optimisation depending on their specific clinical or research applications.

## Contrast agents

Gadolinium-based contrast agents (GBCAs) in myocardial $T_1$ mapping are subject to their own issues and controversies for deriving estimates of myocardial ECV. This section discusses the various assumptions made about GBCAs in $T_1$ and ECV mapping.

### Assumptions relating to contrast agents

Several basic assumptions regarding GBCA estimation of ECV are stated here first, with further details later. Strictly, we assume that the contrast agent has identical relaxivities, $r_1$, in myocardium and blood pool:

$$\Delta R_{1,\mathrm{myo}} = r_{1,\mathrm{myo}}[\mathrm{Gd}]_{\mathrm{myo}} \tag{3}$$

$$\Delta R_{1,\mathrm{blood}} = r_{1,\mathrm{blood}}[\mathrm{Gd}]_{\mathrm{blood}}, \tag{4}$$

where $\Delta R_{1,\mathrm{myo}}$ and $\Delta R_{1,\mathrm{blood}}$ are the changes in relaxation rates in myocardium and blood, respectively, and [Gd] represents the concentration of GBCA, typically in millimole/litre units [75, 76]. The change in relaxation rate, $\Delta R_1$, is given as:

$$\Delta R_1 = \left(1/T_1\right)_{\mathrm{postGad}} - \left(1/T_1\right)_{\mathrm{native}}. \tag{5}$$

If we assume that $r_{1,\mathrm{myo}} = r_{1,\mathrm{blood}}$, as stated above, then:

$$\Delta R_1 = r_1[\mathrm{Gd}] \rightarrow \Delta R_{1,\mathrm{myo}} / \Delta R_{1,\mathrm{blood}} = [\mathrm{Gd}]_{\mathrm{myo}} / [\mathrm{Gd}]_{\mathrm{blood}}, \tag{6}$$

where the ratio $[\mathrm{Gd}]_{\mathrm{myo}} / [\mathrm{Gd}]_{\mathrm{blood}}$ is the partition coefficient, $\lambda$ [75, 77].

Secondly, we assume that the GBCA does not enter myocytes or blood cells, and that it is instead in dynamic equilibrium of water relaxation inside those cells, because of fast-exchange of water through cell walls, as follows:

$$[\mathrm{Gd}]_{\mathrm{myo}} = [\mathrm{Gd}]_{\mathrm{interstitial}} \times \mathrm{ECV} \tag{7}$$

$$[\mathrm{Gd}]_{\mathrm{blood}} = [\mathrm{Gd}]_{\mathrm{bl\_plasma}} \times (1 - \mathrm{Hct}), \tag{8}$$

where Hct is the haematocrit. The term "fast" implies fast exchange of enough water across cell walls relative to the relevant $T_1$ range late after the myocardial first-pass.

Both amyloid deposition and collagen accumulation in fibrosis increase the interstitial space and break up myocyte packing. Collagen itself is of negligible non-permeated or "dark" volume (very short $T_2$), and is assumed to be highly permeable to interstitial fluid, including the GBCA. If the GBCA did not enter the collagen volume, but achieved relaxation equilibrium with it by fast exchange, it would manifest as an abnormally low ECV, resembling myocyte hypertrophy.

Finally, late after injection we assume that the concentration of GBCA in the interstitial fluid is equal to that in the blood plasma [77], and we calculate ECV as follows:

$$[\mathrm{Gd}]_{\mathrm{interstitial}} = [\mathrm{Gd}]_{\mathrm{bl\_plasma}} \rightarrow \mathrm{ECV} = (1 - \mathrm{Hct}) \times \Delta R_{1,\mathrm{myo}} / \Delta R_{1,\mathrm{blood}}, \tag{9}$$

as described by Messroghli et al. [78].

### Contrast agent types

Several GBCAs are available for $T_1$ mapping applications, including gadopentetate dimeglumine (Gd-DTPA), gadobenate dimeglumine (Gd-BOPTA), and gadobutrol; these are known under the trade names "Magnevist", "Multihance", and "Gadovist", respectively. Each agent has differing relaxivities and binding properties, which can lead to differences in the estimated ECV; further complications arise due to relaxivity variations with different field strengths.

The Gd-BOPTA agent's aromatic ring enables weak plasma protein binding, leading to a lower molecular tumbling rate and thus a longer rotational MR correlation time and higher relaxivity in blood plasma and myocardial interstitial fluid compared to Gd-DTPA and gadobutrol. Furthermore, a lower dose of Gd-BOPTA has been shown to have similar diagnostic efficacy to a higher dose of Gd-DTPA in LGE imaging of MI [79]. Kawel et al. have shown that the use of Gd-DTPA leads to myocardial $T_1$ values around 15 ms lower than Gd-BOPTA, with no statistically significant difference seen in blood pool [80]. This results in slightly greater ECV values measured by Gd-DTPA,

of the order of 0.01, perhaps due to Gd-BOPTA's binding to human serum albumin, which is responsible for its increased relaxivity. With regards to relaxivity variations with field strength, work by Rohrer et al. and Pintaske et al. has illustrated the variability in $R_1$ of GBCAs in human blood plasma for different contrast agent types and at different field strengths [81, 82], which will lead to bias and variability in ECV measurements if not accounted for.

The relatively greater presence of albumin in blood versus myocardium means the distribution of protein-bound contrast agent between these pools is likely to be different than for non-protein-bound equivalents, altering the ratio of the change in relaxation rate of myocardium and blood and thus altering ECV. Given that this distorts one of the assumptions of in gadolinium-based ECV estimation, use of a protein-bound contrast agent will slightly modify partition coefficient estimation by $T_1$ mapping. If investigators plan to use one of these agents, they should do so consistently, and report this clearly in any inter-site comparisons.

### Steady-state contrast versus bolus administration

The method of contrast administration also introduces variability to ECV calculation. Under most conditions, the two-compartment steady-state assumption, stated in Eq. (9), holds true for single bolus administration [83–85]. Early work in ECV used a primed infusion approach, whereby an initial loading bolus is followed by a continuous infusion of GBCA [86]. For most situations, the simpler bolus-only approach gives a similar ECV; however, for ECV greater than 0.4, in myocardial infarction (MI) and amyloidosis for example [87], it substantially overestimates ECV [84]. In a third method, several $T_1$ mapping acquisitions can be acquired during GBCA washout for improved accuracy in estimating the gadolinium blood-myocardium partition coefficient [24, 88, 89], which is estimated through the slope of a linear fit to myocardial $R_1$ versus blood $R_1$. The partition coefficient has been shown to deviate from this model in the early washout phase [90, 91], causing underestimation of ECV. This can be seen in Fig. 5, where data become markedly non-linear for blood $R_1$ values greater than 4 $s^{-1}$; these data are often excluded from ECV calculations to avoid bias (Jerosch-Herold, personal communication).

### Fast exchange assumption

Equations (7) and (8) are dependent on the fast exchange assumption, whereby we assume that water exchange between intracellular and extracellular compartments is sufficiently fast relative to the difference between the relaxation rates of the compartments considered in isolation [75]. In cases where this assumption is broken, where higher GBCA concentrations are used or post-GBCA measurements are made too early, as discussed above, ECV may be underestimated [92]. Regardless, in typical clinical $T_1$-mapping situations, it appears that the fast-exchange assumption is sound.

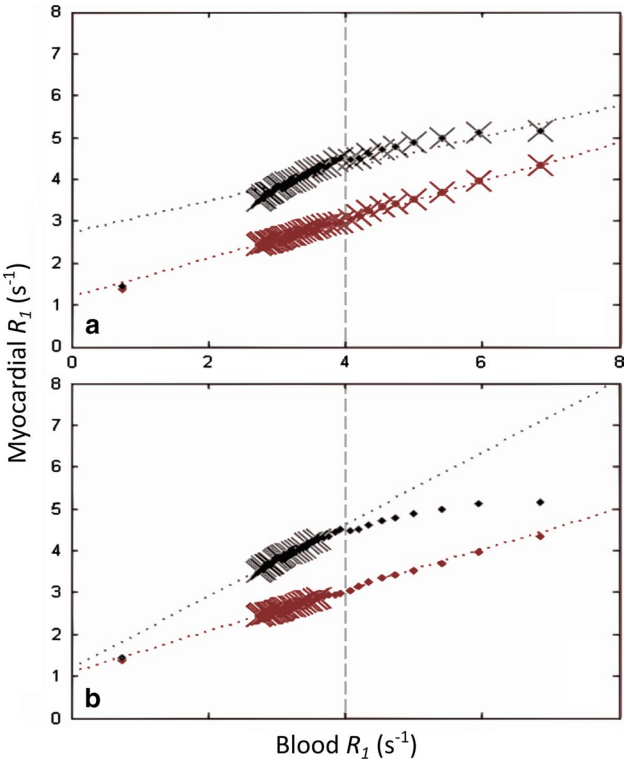


**Fig. 5** Estimation of partition coefficient in chronic myocardial infarction patients. *Plots* show myocardial relaxation rate ($R_1$) versus blood $R_1$ in viable and infarcted myocardium (*red* and *black points*, respectively) for two different post-contrast serial acquisition schemes. Note that the slopes of the linear regressions (partition coefficients, λ, indicated by *dotted lines*) change considerably depending on the sampled points (*crosses*) for infarcted tissue, but remain relatively constant in viable myocardium. *Plot* (**a**) used time points from 1 to 40 min for partition coefficient estimation, which gave $\lambda = 0.46$ in viable myocardium and 0.38 in infarct. *Plot* (**b**) used time points from 15 to 40 min for linear regression, leading to $\lambda = 0.49$ in viable tissue and 0.86 in infracted tissue. *Dashed grey lines* indicate the cut-off $R_1$ of 4 $s^{-1}$, above which points are generally excluded to avoid nonlinearity of λ (Jerosch-Herold, personal communication). Adapted with permission from Goldfarb and Zhao [90]

### Use of blood $T_1$ to calculate haematocrit

The blood for haematocrit assessment should be taken contemporaneously with $T_1$ mapping [13], to avoid unnecessary scatter in ECV. Synthetic haematocrit has recently been proposed as a means of streamlining ECV calculation [93]; it is calculated using the linear relationship between native blood $T_1$ and blood-analysed haematocrit. Support for this approach is spreading [93, 94]; however, several issues have been identified that should be considered [95, 96].

### Summary of contrast agent issues

Although there are multiple issues with contrast agent types and field-strengths, none of these appear to dominate. There perhaps remains a dilemma between optimal ECV assessment and clinical feasibility: for example, the use of multiple acquisitions during GBCA washout, along with multiple averages for native $T_1$ scans, will improve ECV accuracy and precision, but such a protocol is difficult to fit into busy clinical schedules.

## Errors in specific clinical applications

The aim of this section is to highlight the impact of the above topics in specific clinical applications, with examples and possible solutions.

### Differences in age, sex, and myocardial region

There appear to be subtle differences in native myocardial $T_1$ related to sex and age, though there is currently no consensus on whether these also influence ECV [28, 64, 97–99]. Several investigators have posited theories as to why native $T_1$ and ECV might increase or decrease with age, but the debate over these issues is outside the scope of this review. We should, however, point out that these changes are small, and demonstrable only over large groups, with a similar scatter to $T_1$ and ECV estimates in diffuse fibrosis, which are discussed later.

Regarding myocardial region, there appears to be no statistically significant difference between native $T_1$ measurements in the basal, mid, and apical regions of the left ventricle in healthy volunteers [100]. Several studies, however, have reported lower native $T_1$ values in the lateral wall versus the inter-ventricular septum [30, 64, 68, 97, 101]. It is likely this is mainly due to technical confounds rather than physiological differences, as cardiac motion, off-resonance by local $B_0$ distortion, and lower coil sensitivity all reduce accuracy and precision in the lateral wall. ECV, on the other hand, does not differ significantly between the lateral wall and septum [97], suggesting that reduction of native $T_1$ by off-resonance is likely the main source. Figure 6 illustrates the variation of native $T_1$ throughout the heart; lower $T_1$ values are seen in inferolateral segments, which typically demonstrate off-resonance due to interfaces with the lung and the posterior vein of the left ventricle [102, 103].

### Routine clinical applications of $T_1$ and ECV mapping

Myocardial $T_1$ and ECV mapping has attracted a lot of interest for both clinical and research applications due to its potential for accurate and precise tissue characterisation on a pixel-by-pixel basis. While $T_1$ mapping still shows promise for aiding precision medicine and influencing management of individual patients, recent work has been more pragmatic, with applications focusing on large patient populations and specific conditions.

#### *Cardiac amyloidosis*

Amyloid is a relatively rare multi-system condition where deposition of misfolded fibrillary protein in tissues and organs can cause expansion of the myocardial extracellular space and impairment of cardiac function [104]. This strongly increases native $T_1$ and ECV globally, with minimal overlap with healthy ranges [84], making them an excellent diagnostic tool [105]. Post-contrast $T_1$ mapping can also be helpful in highlighting abnormal GBCA washout kinetics, which show a specific pattern in amyloid patients [106], and a higher ECV in this context indicates a worse prognosis [107]. With large global changes and no concerns regarding myocardial region, this combination enables $T_1$ mapping to deliver strong diagnostic and prognostic utility.

#### *Anderson-Fabry disease*

Another rare multi-system syndrome, Anderson-Fabry disease (AFD) is characterised by intracellular accumulation of glycosphingolipids. This leads to progressive cardiac, renal, and cerebrovascular disease [108], and thus early diagnosis is extremely important for timely intervention. AFD markedly reduces global myocardial native $T_1$ compared to healthy volunteers, and thus represents a strong application of native $T_1$ mapping [109–111], again without concerns about regional myocardial differences. For several reasons, the reduced global native $T_1$ in AFD likely does not result directly from the short $T_1$ of fat [109], contrasting with apparent local $T_1$ increases sometimes seen in fatty infiltration of chronic MI, which is discussed later.

#### *Myocarditis and Takotsubo cardiomyopathy*

Myocarditis and Takotsubo cardiomyopathy are also potential clinical applications for $T_1$ mapping [112, 113], being characterised by myocardial oedema, among several other markers. Oedema can be clearly highlighted on native $T_1$ maps due to increased interstitial fluid content; indeed, native $T_1$ mapping has higher diagnostic accuracy for identifying oedema than $T_2$-weighted imaging in Takotsubo [113, 114], and myocarditis [115]. In this application, although native $T_1$ is strongly increased, this is often sharply localised in myocardium, and thus operators should take care to localise to the relevant myocardial region. Furthermore, understanding

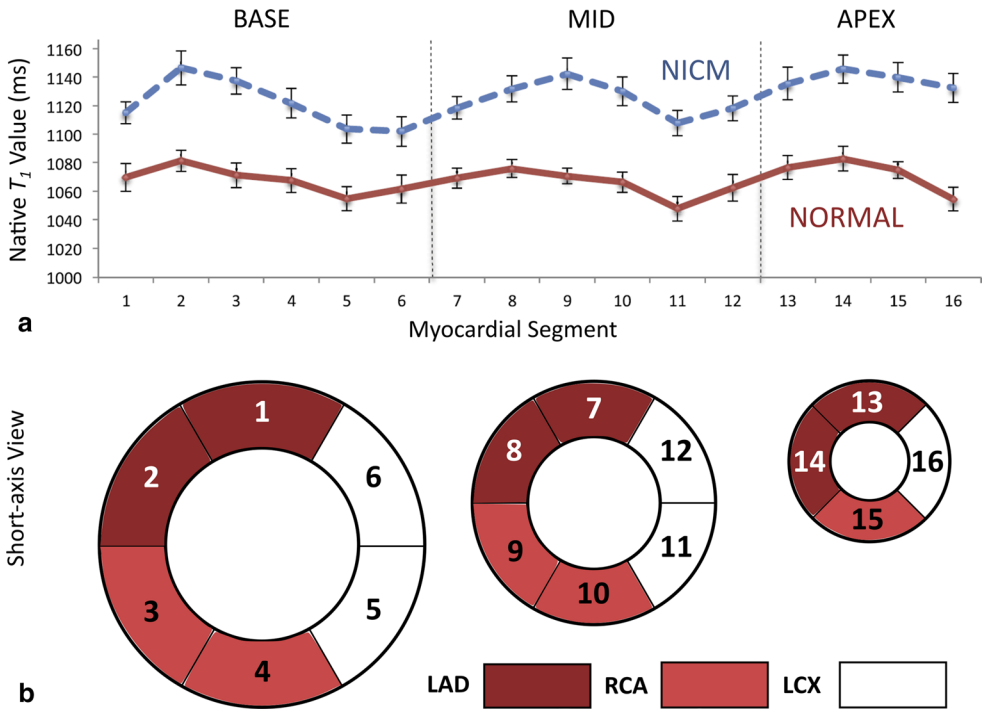


**Fig. 6** Regional variation in native $T_1$ estimates. Graph (**a**) shows variability in segmental native $T_1$ across 16 myocardial segments in subjects with normal left ventricular function (*solid red line*, $n = 27$) versus subjects with non-ischemic cardiomyopathy (*dashed blue line*, $n = 39$). *Error bars* represent the standard error of the mean. Base, mid, and apex refer to levels of the left ventricular myocardium, and segments 2, 3, 8, 9, and 14 are septal, as illustrated by the American Heart Association model (**b**). Inferolateral segments show the lowest native $T_1$ values, likely due to off-resonance at interfaces with the lung and the posterior vein of the left ventricle. The approximate territories of the right coronary artery (RCA) and the left anterior descending (LAD) and left circumflex (LCX) arteries are also shown for interest. Graph (**a**) is reproduced with permission from Shah et al. (2016) Am J Cardiol 117(2): 282–288

of localised technical pitfalls is also valuable: such as off-resonance, whose impact is further modulated by $B_1$ changes over the heart. It should be noted that published studies have typically excluded patients with major epicardial coronary disease or past MI. For $T_1$ mapping to become clinically meaningful in myocarditis and Takotsubo, it should not only positively confirm the diagnosis, but also rule out acute MI.

## Potential clinical applications of $T_1$ mapping

In some pathologies, $T_1$ and ECV currently demonstrate limited sensitivity, but may ultimately be of clinical utility if their precision is improved, or if confounds are addressed.

### *Acute myocardial infarction*

Like myocarditis and Takotsubo, acute MI also presents with oedema, which leads to elevated local $T_1$ on native $T_1$ maps [116–118]. There are, however, potential $T_1$ mapping pitfalls in acute MI, additional to that of local disease. Firstly, microvascular obstruction, or the "no reflow" phenomenon [119], causes derangement of the microvasculature, limiting blood flow post-reperfusion. This can distort an earlier assumption for ECV derivation, that of GBCA equilibrium between the infarct zone and the blood plasma. In particular, the necrotic core of the infarct will not be in equilibrium 15–20 min post-bolus, requiring infusion for accurate ECV measurement [84].

Secondly, myocardial haemorrhage often occurs concomitantly with microvascular obstruction [120], and is characterised by extravasation of red blood cells through gaps in the endothelial walls. This leads to a cascade of haemoglobin decay products in the no reflow region during the weeks following reperfusion, with various iron states affecting $T_2$, estimated $T_1$, and true $T_1$ [121]. Clearly this poses problems for $T_1$ mapping, and thus CMR studies should be timed appropriately after reperfusion therapy [122].

### *Chronic myocardial infarction*

For $T_1$ mapping, chronic MI presents the challenge of lipomatous metaplasia, which affects around 24–47% of MI patients [29, 123]. This is characterised by fatty infiltration

of myocardium, highlighting the following technical difficulty with fat partial volume in $T_1$ mapping.

Ignoring bSSFP characteristics, a mixture of in-phase lipid and water signals within a voxel produces a biexponential $T_1$ recovery curve. Attempting to fit these data with a monoexponential curve typically leads to lower myocardial $T_1$ estimates due to inclusion of short $T_1$ lipids, which have $T_1$ values around 370 ms at 1.5T and 450 ms at 3T [124]. However, in myocardial $T_1$ mapping the mono- versus bi-exponential "model mismatch" issue is usually not the dominant factor, because most $T_1$ mapping uses bSSFP, in which fat and water are typically out of phase due to the frequency offset of fat [125]. Complex interference between fat and water signals leads to counterintuitive results: for smaller fat fractions, around 0.5–40% [29, 126], an increase in the apparent myocardial $T_1$ occurs; higher fat fractions lead to undefined $T_1$ estimates; and fat-like $T_1$ values are seen only at the highest fat fractions. In chronic MI, fat fractions typically do not exceed 35% [29], and thus a positive $T_1$ estimation bias is expected, assuming fat and water are out of phase. This reduces the specificity of native $T_1$ mapping in chronic MI, because similar, but genuine, changes occur in oedema or inflammation. It is currently unclear what effect fatty changes have on ECV. See Fig. 7 for a plot of water and fat signals in bSSFP, along with a native $T_1$ map acquired in a chronic MI patient with lipomatous metaplasia.

The complex impact of fat partial volume in $T_1$ mapping might only reliably be reduced by replacing bSSFP with spoiled GRE imaging, in which the fat phase-difference depends purely on the TE. However, the reduced SNR of spoiled GRE relative to bSSFP would have to be considered. Alternatively, quantitative myocardial fat-fraction mapping could be applied [127], as recent work has incorporated fat–water separation into MOLLI and SASHA $T_1$ mapping in skeletal muscle [128] and the heart [32].

### *Diffuse myocardial fibrosis*

Several pathologies cause diffuse fibrosis of the myocardium, such as hypertrophic and dilated cardiomyopathies (HCM and DCM), atrial fibrillation, aortic stenosis, heart failure with reduced or preserved ejection fractions (HFrEF and HFpEF), congenital heart disease, hypertension [129], and diabetes [130]. Certain drug therapies, such as alkylating agents in chemotherapy, can also lead to diffuse fibrosis [131], and possibly benefit from applications of $T_1$ mapping [132].

In general, native $T_1$ values are increased in diffuse fibrosis, but not to as great an extent as in oedema or amyloidosis, and ECV is also slightly elevated. In general, scatter in estimated $T_1$ values seems to be of a similar order to that seen in diffuse-fibrosis changes, and this has delayed the wider uptake of $T_1$ mapping. Several investigators have shown the usefulness of ECV as a prognostic indicator [133, 134], but there seems to be little progress in taking this towards a per-patient test. In many applications there is a mixture of focal and diffuse fibrosis, which begs the question whether visible focal fibrosis was excluded from ROIs used in diffuse fibrosis studies [135], and even if so, what "mesoscopic" or "microscar" subvoxel focal fibrosis, or other myocardial changes, might be included in the so-called diffuse fibrosis assessment by $T_1$ [136] (Fig. 8).

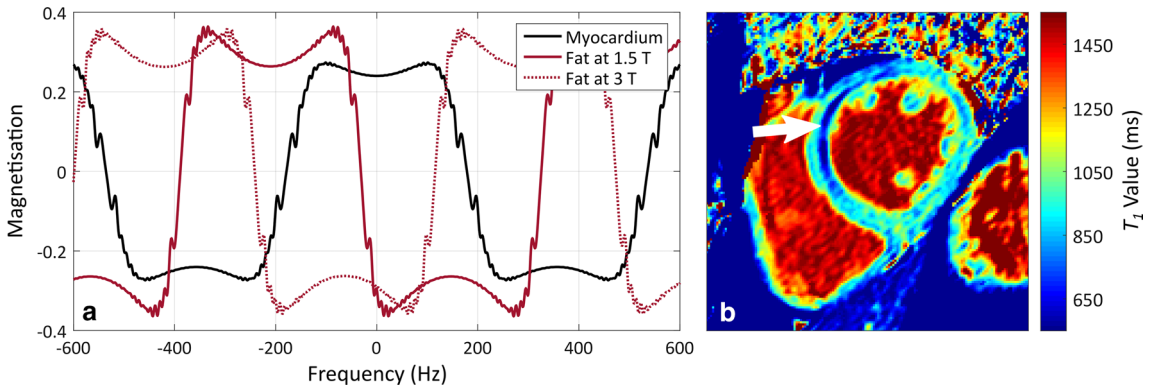


**Fig. 7** The effect of intramyocardial lipids on native $T_1$ estimation in chronic myocardial infarction. The balanced steady-state free-precession off-resonance response is shown for myocardium and fat (**a**), for a modified Look–Locker inversion recovery protocol with a repetition time of 2.8 ms and a flip-angle of 35°. When fat and water are out of phase, lipids typically show an elevated $T_1$ in $T_1$ maps; when they are in-phase, lipid $T_1$ typically appears *lower* than myocardial $T_1$. An example native $T_1$ map (**b**), acquired at 1.5T in a chronic myocardial infarction patient with lipomatous metaplasia, shows a reduced apparent $T_1$ associated with lipid signals (*white arrow*). Both the accuracy and precision of native $T_1$ estimates are influenced by this effect. Figure (**b**) was provided courtesy of Dr Heerajnarain Bulluck, The Hatter Cardiovascular Institute, University College London

Clearly there is substantial overlap between native $T_1$ and ECV values measured in controls versus those measured in patients with likely diffuse fibrosis. This is partly due to the small changes seen in diffuse fibrosis, particularly early in the disease when reversing it would be of great clinical benefit before irreversible damage occurs to the myocardium. It is also related to the many sources of dispersion in $T_1$ parameter estimation. As yet, it appears that there is no one factor that can be adjusted to achieve adequate $T_1$ estimation precision for detecting early diffuse fibrosis. Many recently reported clinical studies naturally retained older $T_1$ mapping protocols, due to the constraints of their study length, or follow-up periods in the "prognosis" papers. Despite these problems on the individual level, which may be overcome by stricter control of errors, $T_1$ mapping of diffuse fibrosis offers concrete benefits in large-scale studies: offering a means of testing treatment effects and characterising differences on a population level [130, 137].

### Summary of clinical sources of error

Both native $T_1$ and ECV are important clinical measures that allow us to characterise the myocardium in a fashion complementary to LGE. The substantial overlap of these measures between patients and controls in some cardiac conditions offers challenges to the clinical use of $T_1$ mapping, at least with current methodology. However, in specific conditions, such as amyloid and Anderson-Fabry disease, $T_1$ mapping has an important diagnostic and prognostic role, and is being widely adopted into routine clinical use.

## Future directions of $T_1$ and ECV mapping

Potential future solutions for errors in $T_1$ and ECV mapping have been discussed throughout this review. We will now highlight several promising areas of development that may determine the future directions of the field.

Free-breathing $T_1$ mapping would appear to offer major gains with regards to $T_1$ mapping accuracy and precision, as well as enabling scanning of patients with compromised breath-holding. There are already several publications demonstrating the benefits of free-breathing $T_1$ mapping [36–39]; however, the added time required for these methods will limit their wider uptake, unless retrospective image registration can be robustly applied.

Certain recent implementations of myocardial $T_1$ mapping have incorporated simulations to improve the accuracy of bSSFP MOLLI [41, 138, 139], to enable spoiled GRE $T_1$ mapping [59], and to reduce the number of pause intervals between Look–Locker sets [140]. As yet, these methods do not offer an advantage in precision over the original MOLLI implementation, but further work may demonstrate benefits to their use [138].

Simultaneous $T_1$, $T_2$, and proton density mapping of the myocardium is also possible [141–144], with some methods being feasible in a single breath-hold [142–144]. Magnetic resonance fingerprinting is an extension of simulation-based methods that can offer $T_1$, $T_2$, and proton density maps [145], as well as other parameters modelled in the dictionary. It has recently been adapted to the heart [146]; however, further work is required, as currently it shows

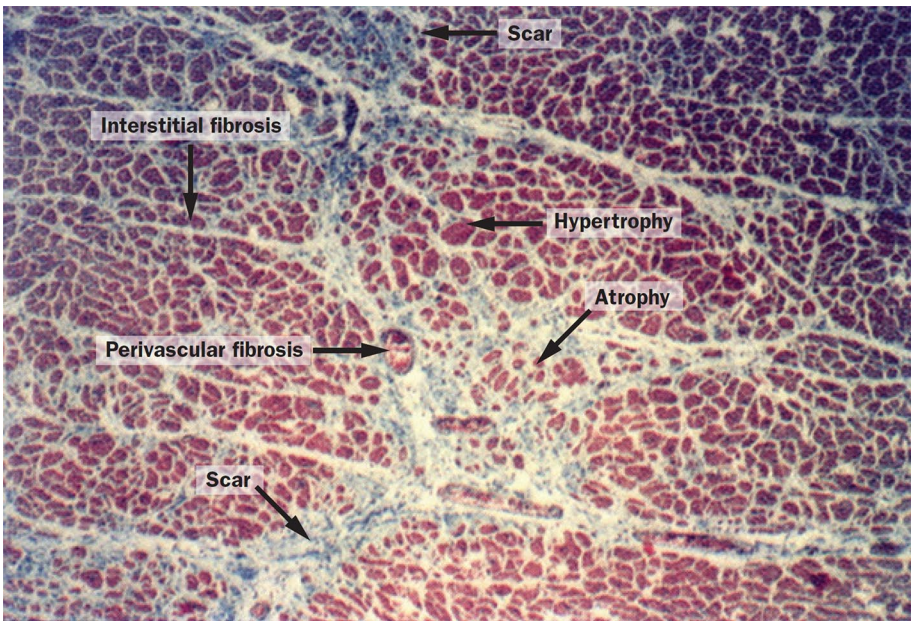


**Fig. 8** Structural remodelling of myocardium in hypertension. Subvoxel heterogeneity can be seen in cardiomyocyte size, which ranges from hypertrophied to atrophied, and in fibrosis, which consists of microscopic scars, and perivascular and interstitial fibrosis. Reproduced with permission from Weber et al. [136]

inferior precision to conventional $T_1$ mapping and requires long computation times for pattern matching.

## Sacrificing $T_1$ accuracy for increased clinical utility

Placing a particular $T_1$ estimate in a local normal range may necessitate high precision, but not high accuracy. Indeed, accuracy may be sacrificed deliberately to yield $T_1$ estimates that are better able to discriminate normal tissue from pathology. For example, increasing the MOLLI excitation flip angle to 50° increases sensitivity to off-resonance, which reduces $T_1$ accuracy, but also increases MT effects, which differ between tissue types. This appears effective in detecting diffuse fibrosis in the septum [30, 147]. The accuracy of this approach is limited, but the "true" $T_1$ is less relevant if local normal ranges are used, as they should be for any $T_1$ mapping implementation, under current guidelines [13].

Conversely, accuracy is important for establishing myocardial $T_1$ and ECV as clinical biomarkers using normal ranges that are transferable between sites and vendors [148].

## Summary

This review has discussed reasons for inaccuracy and imprecision in $T_1$ and ECV mapping, and it should be clear from these considerations that users should take great care when deviating from manufacturers' advised $T_1$ mapping protocols. While improving the apparent quality of maps and source images, users may inadvertently reduce the precision of $T_1$ estimates, damaging clinical utility. Whatever $T_1$ mapping setup is used, it is essential that its performance is characterised in local normal ranges, and that it is applied only for those clinical questions that its precision can support. Ongoing quality control and reassessment is also required to ensure a local normal range remains valid; the reader is referred to the upcoming SCMR and EACVI consensus for recommendations in this regard.

In the research and clinical applications described here, current native $T_1$ and ECV mapping methods show utility in groupwise comparisons through to individual clinical tests. For some conditions, like diffuse fibrosis, mapping methods serve as weakly prognostic biomarkers that might be beneficial in combination with other diagnostic information about an individual patient. In other, albeit quite rare, conditions native $T_1$ and ECV mapping can provide strong diagnostic data.

Fundamentally, cardiac mapping methods have not changed radically since Messroghli et al. first introduced MOLLI [1]; however, their diversity offers challenges to inter-centre use, and new developments and quality controls are still evolving. New approaches that incorporate various forms of undersampling and modelling, such as fingerprinting, do not currently offer substantial gains in accuracy and precision, other than avoiding dependence on breath-holding in some cases.

It remains unclear how much of the scatter observed in $T_1$ estimates is due to physiological differences in true $T_1$, or how much might be eliminated if the potentially correctable issues discussed here could be addressed robustly. If these pitfalls can be accounted for simply, quickly, and reliably, without need for specialist attention, $T_1$ and ECV mapping may ultimately support more widespread clinical applications.

#### Compliance with ethical standards

**Conflict of interest** The authors declare that they have no conflict of interest.



## References

1. Messroghli DR, Radjenovic A, Kozerke S, Higgins DM, Sivananthan MU, Ridgway JP (2004) Modified Look–Locker inversion recovery (MOLLI) for high-resolution T1 mapping of the heart. Magn Reson Med 52(1):141–146
2. Kellman P, Wilson JR, Xue H, Bandettini WP, Shanbhag SM, Druey KM, Ugander M, Arai AE (2012) Extracellular volume fraction mapping in the myocardium, part 2: initial clinical experience. J Cardiovasc Magn Reson 14:64
3. Ugander M, Oki AJ, L-y Hsu, Kellman P, Greiser A, Aletras AH, Sibley CT, Chen MY, Bandettini WP, Arai AE (2012) Extracellular volume imaging by magnetic resonance imaging provides insights into overt and sub-clinical myocardial pathology. Eur Heart J 33:1268–1278
4. Kellman P, Arai AE, Xue H (2013) T1 and extracellular volume mapping in the heart: estimation of error maps and the influence of noise on precision. J Cardiovasc Magn Reson 15:56
5. Kellman P, Hansen MS (2014) T1-mapping in the heart: accuracy and precision. J Cardiovasc Magn Reson 16:2
6. Roujol S, Weingärtner S, Foppa M, Chow K, Kawaji K, Ngo LH, Kellman P, Manning WJ, Thompson RB, Nezafat R (2014) Accuracy, precision, and reproducibility of four T1 mapping sequences: a head-to-head comparison of MOLLI, ShMOLLI, SASHA, and SAPPHIRE. Radiology 272(3):683–689
7. Weingärtner S, Meßner NM, Budjan J, Loßnitzer D, Mattler U, Papavassiliu T, Zöllner FG, Schad LR (2016) Myocardial T1-mapping at 3T using saturation-recovery: reference values,

precision and comparison with MOLLI. J Cardiovasc Magn Reson 18(1):84
8. Haaf P, Garg P, Messroghli DR, Broadbent DA, Greenwood JP, Plein S (2016) Cardiac T1 mapping and extracellular volume (ECV) in clinical practice: a comprehensive review. J Cardiovasc Magn Reson 18:89
9. Taylor AJ, Salerno M, Dharmakumar R, Jerosch-Herold M (2016) T1 mapping basic techniques and clinical applications. JACC Cardiovasc Imaging 9(1):67–81
10. Kammerlander AA, Marzluf BA, Zotter-Tufaro C, Aschauer S, Duca F, Bachmann A, Knechtelsdorfer K, Wiesinger M, Pfaffenberger S, Greiser A, Lang IM, Bonderman D, Mascherbauer J (2016) T1 mapping by CMR imaging from histological validation to clinical implication. JACC Cardiovasc Imaging 9(1):14–23
11. Schelbert EB, Messroghli DR (2016) State of the art: clinical applications of cardiac T1 mapping. Radiology 278(3):658–676
12. Higgins DM, Moon JC (2014) Review of T1 mapping methods: comparative effectiveness including reproducibility issues. Curr Cardiovasc Imaging Rep 7(3):1–10
13. Moon JC, Messroghli DR, Kellman P, Piechnik SK, Robson MD, Ugander M, Gatehouse PD, Arai AE, Friedrich MG, Neubauer S, Schulz-Menger J, Schelbert EB (2013) Myocardial T1 mapping and extracellular volume quantification: a Society for Cardiovascular Magnetic Resonance (SCMR) and CMR Working Group of the European Society of Cardiology consensus statement. J Cardiovasc Magn Reson 15:92
14. Messroghli DR, Greiser A, Fröhlich M, Dietz R, Schulz-Menger J (2007) Optimization and validation of a fully-integrated pulse sequence for modified Look–Locker inversion-recovery (MOLLI) T1 mapping of the heart. J Magn Reson Imaging 26(4):1081–1086
15. Piechnik SK, Ferreira VM, Dall'Armellina E, Cochlin LE, Greiser A, Neubauer S, Robson MD (2010) Shortened modified Look–Locker inversion recovery (ShMOLLI) for clinical myocardial T1-mapping at 1.5 and 3T within a 9 heartbeat breathhold. J Cardiovasc Magn Reson 12:69
16. Chow K, Flewitt JA, Green JD, Pagano JJ, Friedrich MG, Thompson RB (2014) Saturation recovery single-shot acquisition (SASHA) for myocardial T1 mapping. Magn Reson Med 71(6):2082–2095
17. Slavin GS, Hood MN, Ho VB, Stainsby JA (2012) Breath-held myocardial T1 mapping using multiple single-point saturation recovery In: Proceedings of the 20th Annual Meeting of ISMRM, Melbourne, Australia, 1244
18. Higgins DM, Ridgway JP, Radjenovic A, Sivananthan UM, Smith MA (2005) T1 measurement using a short acquisition period for quantitative cardiac applications. Med Phys 32(6):1738–1746
19. Weingärtner S, Akcakaya M, Basha T, Kissinger KV, Goddu B, Berg S, Manning WJ, Nezafat R (2014) Combined saturation/inversion recovery sequences for improved evaluation of scar and diffuse fibrosis in patients with arrhythmia or heart rate variability. Magn Reson Med 71(3):1024–1034
20. Kellman P, Wilson JR, Xue H, Ugander M, Arai AE (2012) Extracellular volume fraction mapping in the myocardium, part 1: evaluation of an automated method. J Cardiovasc Magn Reson 14:63
21. Messroghli DR, Rudolph A, Abdel-Aty H, Wassmuth R, Kühne T, Dietz R, Schulz-Menger J (2010) An open-source software tool for the generation of relaxation time maps in magnetic resonance imaging. BMC Med Imaging 10(1):16
22. Altabella L, Borrazzo C, Carnì M, Galea N, Francone M, Fiorelli A, Di Castro E, Catalano C, Carbone I (2017) A feasible and automatic free tool for T1 and ECV mapping. Phys Med 33:47–55
23. Amano Y, Takayama M, Kumita S (2009) Contrast-enhanced myocardial T1-weighted scout (Look–Locker) imaging for the detection of myocardial damages in hypertrophic cardiomyopathy. J Magn Reson Imaging 30(4):778–784
24. Nacif MS, Turkbey EB, Gai N, Nazarian S, van der Geest RJ, Noureldin RA, Sibley CT, Ugander M, Liu S, Arai AE, Lima JAC, Bluemke DA (2011) Myocardial T1 mapping with MRI: comparison of Look–Locker and MOLLI sequences. J Magn Reson Imaging 34(6):1367–1373
25. Look DC, Locker DR (1969) Pulsed NMR by tone-burst generation. J Chem Phys 50(5):2269–2270
26. Look DC, Locker DR (1970) Time saving in measurement of NMR and EPR relaxation times. Rev Sci Instrum 41(2):250–251
27. Kellman P, Xue H, Chow K, Spottiswoode BS, Arai AE, Thompson RB (2014) Optimized saturation recovery protocols for T1-mapping in the heart: influence of sampling strategies on precision. J Cardiovasc Magn Reson 16:55
28. Piechnik SK, Ferreira VM, Lewandowski AJ, Ntusi NAB, Banerjee R, Holloway C, Hofman MBM, Sado DM, Maestrini V, White SK, Lazdam M, Karamitsos T, Moon JC, Neubauer S, Leeson P, Robson MD (2013) Normal variation of magnetic resonance T1 relaxation times in the human population at 1.5T using ShMOLLI. J Cardiovasc Magn Reson 15:1
29. Kellman P, Bandettini WP, Mancini C, Hammer-hansen S, Hansen MS, Arai AE (2015) Characterization of myocardial T1-mapping bias caused by intramyocardial fat in inversion recovery and saturation recovery techniques. J Cardiovasc Magn Reson 17:33
30. Rogers T, Dabir D, Mahmoud I, Voigt T, Schaeffter T, Nagel E, Puntmann VO (2013) Standardization of T1 measurements with MOLLI in differentiation between health and disease–the ConSept study. J Cardiovasc Magn Reson 15:78
31. Weingärtner S, Meßner NM, Zöllner FG, Akçakaya M, Schad LR (2016) Black-blood native T1 mapping: blood signal suppression for reduced partial voluming in the myocardium. Magn Reson Med. doi:10.1002/mrm.26378
32. Pagano JJ, Chow K, Yang R, Thompson RB (2014) Fat-water separated myocardial T1 mapping with IDEAL-T1 saturation recovery gradient echo imaging. J Cardiovasc Magn Reson 16(Suppl 1):P65
33. Heng EL, Kellman P, Gatzoulis MA, Moon J, Gatehouse P, Babu-Narayan SV (2016) Quantifying right ventricular diffuse fibrosis in tetralogy of Fallot-a novel customised approach for the challenges of the right ventricle. J Cardiovasc Magn Reson 18(Suppl 1):O26
34. Mehta BB, Chen X, Bilchick KC, Salerno M, Epstein FH (2015) Accelerated and navigator-gated Look–Locker imaging for cardiac T1 estimation (ANGIE): development and application to T1 mapping of the right ventricle. Magn Reson Med 73(1):150–160
35. Wang X, Joseph AA, Kalentev O, Merboldt K-D, Voit D, Roeloffs VB, van Zalk M, Frahm J (2016) High-resolution myocardial T1 mapping using single-shot inversion recovery fast low-angle shot MRI with radial undersampling and iterative reconstruction. Br J Radiol 89(1068):20160255
36. Tsai J-M, Huang T-Y, Tseng Y-S, Lin Y-R (2012) Free-breathing MOLLI: application to myocardial T1 mapping. Med Phys 39(101):7291–7302
37. Weingärtner S, Akcakaya M, Roujol S, Basha T, Stehning C, Kissinger KV, Goddu B, Berg S, Manning WJ, Nezafat R (2015) Free-breathing post-contrast three-dimensional T1 mapping: volumetric assessment of myocardial T1 values. Magn Reson Med 73(1):214–222
38. Weingärtner S, Roujol S, Akcakaya M, Basha TA, Nezafat R (2015) Free-breathing multislice native myocardial T1 mapping

using the slice-interleaved T1 (STONE) sequence. Magn Reson Med 74(1):115–124
39. Chow K, Yang Y, Shaw P, Kramer CM, Salerno M (2016) Robust free-breathing SASHA T1 mapping with high-contrast image registration. J Cardiovasc Magn Reson 18:47
40. Kellman P, Herzka DA, Hansen MS (2014) Adiabatic inversion pulses for myocardial T1 mapping. Magn Reson Med 71(4):1428–1434
41. Shao J, Nguyen KL, Natsuaki Y, Spottiswoode B, Hu P (2015) Instantaneous signal loss simulation (InSiL): an improved algorithm for myocardial T1 mapping using the MOLLI sequence. J Magn Reson Imaging 41(3):721–729
42. Rodgers CT, Piechnik SK, DelaBarre LJ, Moortele PF, Snyder CJ, Neubauer S, Robson MD, Vaughan JT (2013) Inversion recovery at 7T in the human myocardium: measurement of T1, inversion efficiency and B1+. Magn Reson Med 70(4):1038–1046
43. Gai ND, Stehning C, Nacif M, Bluemke DA (2013) Modified Look–Locker T1 evaluation using Bloch simulations: human and phantom validation. Magn Reson Med 69(2):329–336
44. Chow K, Kellman P, Spottiswoode BS, Nielles-Vallespin S, Arai AE, Salerno M, Thompson RB (2015) Saturation pulse design for quantitative myocardial T1 mapping. J Cardiovasc Magn Reson 17:84
45. Mueller A, Kouwenhoven M, Naehle CP, Gieseke J, Strach K, Willinek WA, Schild HH, Thomas D (2012) Dual-source radiofrequency transmission with patient-adaptive local radiofrequency shimming for 3.0-T cardiac MR imaging: initial experience. Radiology 263(1):77–85
46. Malik SJ, Larkman DJ, Hajnal JV (2009) Optimal linear combinations of array elements for B1 mapping. Magn Reson Med 62(4):902–909
47. Robson MD, Piechnik SK, Tunnicliffe EM, Neubauer S (2013) T1 measurements in the human myocardium: the effects of magnetization transfer on the SASHA and MOLLI sequences. Magn Reson Med 70(3):664–670
48. Kellman P, Da Herzka, Arai AE, Hansen M (2013) Influence of off-resonance in myocardial T1-mapping using SSFP based MOLLI method. J Cardiovasc Magn Reson 15:63
49. Bieri O (2013) Ultra-fast steady state free precession and its application to in vivo 1H morphological and functional lung imaging at 1.5 tesla. Magn Reson Med 70(3):657–663
50. Jung BA, Hennig J, Scheffler K (2002) Single-breathhold 3D-trueFISP cine cardiac imaging. Magn Reson Med 48(5):921–925
51. Deimling M, Heid O (1994) Magnetization prepared true FISP imaging. In: Proceedings of the 2nd Annual Meeting of ISMRM, San Francisco, USA, 495
52. Deshpande VS, Chung YC, Zhang Q, Shea SM, Li D (2003) Reduction of transient signal oscillations in true-FISP using a linear flip angle series magnetization preparation. Magn Reson Med 49(1):151–157
53. Cameron D, Higgins DM, Stehning C, Kouwenhoven M, Bouhrara M, Frenneaux MP, Dawson DK, Redpath TW (2015) Selection of magnetization catalyzation and readout methods for modified Look–Locker inversion recovery: a T1 mapping primer. Magn Reson Imaging 33(4):363–373
54. Chow K, Flewitt JA, Pagano JJ, Green JD, Friedrich MG, Thompson RB (2012) MOLLI T1 values have systematic T2 and inversion efficiency dependent errors. In: Proceedings of the 20th Annual Meeting of ISMRM, Melbourne, Australia, 395
55. Bieri O, Scheffler K (2013) Fundamentals of balanced steady state free precession MRI. J Magn Reson Imaging 38(1):2–11
56. Gruetter R, Tkáč I (2000) Field mapping without reference scan using asymmetric echo-planar techniques. Magn Reson Med 43(2):319–323
57. Schär M, Kozerke S, Fischer SE, Boesiger P (2004) Cardiac SSFP imaging at 3 tesla. Magn Reson Med 51(4):799–806
58. Fillmer A, Kirchner T, Cameron D, Henning A (2015) Constrained image-based $B_0$ shimming accounting for "local minimum traps" in the optimization and field inhomogeneities outside the region of interest. Magn Reson Med 73(4):1370–1380
59. Shao J, Rapacchi S, Nguyen KL, Hu P (2016) Myocardial T1 mapping at 3.0 tesla using an inversion recovery spoiled gradient echo readout and bloch equation simulation with slice profile correction (BLESSPC) T1 estimation algorithm. J Magn Reson Imaging 43(2):414–425
60. Shao J, Rashid S, Renella P, Nguyen K-L, Hu P (2016) Myocardial T1 mapping for patients with implanted cardiac devices using wideband inversion recovery spoiled gradient echo readout. Magn Reson Med 77(4):1495–1504
61. Preibisch C, Deichmann R (2009) Influence of RF spoiling on the stability and accuracy of T1 mapping based on spoiled FLASH with varying flip angles. Magn Reson Med 61(1):125–135
62. Hong KP, Collins J, Lee DC, Wilcox JE, Markl M, Carr J, Kim D (2016) Optimized AIR and investigational MOLLI cardiac T1 mapping pulse sequences produce similar intra-scan repeatability in patients at 3T. NMR Biomed 29(10):1454–1463
63. Bieri O, Markl M, Scheffler K (2005) Analysis and compensation of eddy currents in balanced SSFP. Magn Reson Med 54(1):129–137
64. Dabir D, Child N, Kalra A, Rogers T, Gebker R, Jabbour A, Plein S, C-y Yu, Otton J, Kidambi A, McDiarmid A, Broadbent D, Higgins DM, Schnackenburg B, Foote L, Cummins C, Nagel E, Puntmann VO (2014) Reference values for healthy human myocardium using a T1 mapping methodology: results from the International T1 multicenter cardiovascular magnetic resonance study. J Cardiovasc Magn Reson 16:69
65. Xue H, Shah S, Greiser A, Guetter C, Littmann A, Jolly MP, Arai AE, Zuehlsdorff S, Guehring J, Kellman P (2012) Motion correction for myocardial T1 mapping using image registration with synthetic image estimation. Magn Reson Med 67(6):1644–1655
66. Ferreira VM, Wijesurendra RS, Liu A, Greiser A, Casadei B, Robson MD, Neubauer S, Piechnik SK (2015) Systolic ShMOLLI myocardial T1-mapping for improved robustness to partial-volume effects and applications in tachyarrhythmias. J Cardiovasc Magn Reson 17:77
67. Zhao L, Li S, Ma X, Greiser A, Zhang T, An J, Bai R, Dong J, Fan Z (2016) Systolic MOLLI T1 mapping with heart-rate-dependent pulse sequence sampling scheme is feasible in patients with atrial fibrillation. J Cardiovasc Magn Reson 18:13
68. Kawel N, Nacif M, Zavodni A, Jones J, Liu S, Sibley CT, Bluemke DA (2012) T1 mapping of the myocardium: intra-individual assessment of the effect of field strength, cardiac cycle and variation by myocardial region. J Cardiovasc Magn Reson 14:27
69. Fitts M, Breton E, Kholmovski EG, Dosdall DJ, Vijayakumar S, Hong KP, Ranjan R, Marrouche NF, Axel L, Kim D (2013) Arrhythmia insensitive rapid cardiac T1 mapping pulse sequence. Magn Reson Med 70(5):1274–1282
70. Tong CY, Prato FS (1994) A novel fast T1-mapping method. J Magn Reson Imaging 4(5):701–708
71. Huang TY, Tseng YS, Chuang TC (2014) Automatic calibration of trigger delay time for cardiac MRI. NMR Biomed 27(4):417–424
72. Cain PA, Ahl R, Hedstrom E, Ugander M, Allansdotter-Johnsson A, Friberg P, Arheden H (2009) Age and gender specific normal values of left ventricular mass, volume and function for gradient echo magnetic resonance imaging: a cross sectional study. BMC Med Imaging 9(1):2

73. Bieri O, Scheffler K (2006) On the origin of apparent low tissue signals in balanced SSFP. Magn Reson Med 56(5):1067–1074
74. Stanisz GJ, Odrobina EE, Pun J, Escaravage M, Graham SJ, Bronskill MJ, Henkelman RM (2005) T1, T2 relaxation and magnetization transfer in tissue at 3T. Magn Reson Med 54(3):507–512
75. Donahue KM, Burstein D, Manning WJ, Gray ML (1994) Studies of Gd-DTPA relaxivity and proton exchange rates in tissue. Magn Reson Med 32(1):66–76
76. Flacke SJ, Fischer SE, Lorenz CH (2001) Measurement of the gadopentetate dimeglumine partition coefficient in human myocardium in vivo: normal distribution and elevation in acute and chronic infarction. Radiology 218(3):703–710
77. Arheden H, Saeed M, Higgins CB, Gao D-W, Bremerich J, Wyttenbach R, Dae MW, Wendland MF (1999) Measurement of the distribution volume of gadopentetate dimeglumine at echo-planar MR imaging to quantify myocardial infarction: comparison with 99mTc-DTPA autoradiography in rats. Radiology 211(3):698–708
78. Messroghli DR, Nordmeyer S, Dietrich T, Dirsch O, Kaschina E, Savvatis K, Klein C, Berger F, Kuehne T (2011) Assessment of diffuse myocardial fibrosis in rats using small-animal Look–Locker inversion recovery T1 mappingclinical perspective. Circ Cardiovasc Imaging 4(6):636–640
79. Balci NC, Inan N, Anik Y, Erturk MS, Ural D, Demirci A (2006) Low-dose gadobenate dimeglumine versus standard-dose gadopentate dimeglumine for delayed contrast-enhanced cardiac magnetic resonance imaging. Acad Radiol 13(7):833–839
80. Kawel N, Nacif M, Zavodni A, Jones J, Liu S, Sibley CT, Da Bluemke (2012) T1 mapping of the myocardium: intra-individual assessment of post-contrast T1 time evolution and extracellular volume fraction at 3T for Gd-DTPA and Gd-BOPTA. J Cardiovasc Magn Reson 14:26
81. Rohrer M, Bauer H, Mintorovitch J, Requardt M, Weinmann H-J (2005) Comparison of magnetic properties of MRI contrast media solutions at different magnetic field strengths. Invest Radiol 40(11):715–724
82. Pintaske J, Martirosian P, Graf H, Erb G, Lodemann K-P, Claussen CD, Schick F (2006) Relaxivity of gadopentetate dimeglumine (Magnevist), gadobutrol (Gadovist), and gadobenate dimeglumine (MultiHance) in human blood plasma at 0.2, 1.5, and 3 tesla. Invest Radiol 41(3):213–221
83. Schelbert EB, Testa SM, Meier CG, Ceyrolles WJ, Levenson JE, Blair AJ, Kellman P, Jones BL, Ludwig DR, Schwartzman D (2011) Myocardial extravascular extracellular volume fraction measurement by gadolinium cardiovascular magnetic resonance in humans: slow infusion versus bolus. J Cardiovasc Magn Reson 13:16
84. White SK, Sado DM, Fontana M, Banypersad SM, Maestrini V, Flett AS, Piechnik SK, Robson MD, Hausenloy DJ, Sheikh AM (2013) T1 mapping for myocardial extracellular volume measurement by CMR: bolus only versus primed infusion technique. JACC Cardiovasc Imaging 6(9):955–962
85. Salerno M, Janardhanan R, Jiji RS, Brooks J, Adenaw N, Mehta B, Yang Y, Antkowiak P, Kramer CM, Epstein FH (2013) Comparison of methods for determining the partition coefficient of gadolinium in the myocardium using T1 mapping. J Magn Reson Imaging 38(1):217–224
86. Flett AS, Hayward MP, Ashworth MT, Hansen MS, Taylor AM, Elliott PM, McGregor C, Moon JC (2010) Equilibrium contrast cardiovascular magnetic resonance for the measurement of diffuse myocardial fibrosis: preliminary validation in humans. Circulation 122(2):138–144
87. Sado DM, Flett AS, Banypersad SM, White SK, Maestrini V, Quarta G, Lachmann RH, Murphy E, Mehta A, Hughes DA (2012) Cardiovascular magnetic resonance measurement of myocardial extracellular volume in health and disease. Heart 98:1436–1441
88. Jerosch-Herold M, Sheridan DC, Kushner JD, Nauman D, Burgess D, Dutton D, Alharethi R, Li D, Hershberger RE (2008) Cardiac magnetic resonance imaging of myocardial contrast uptake and blood flow in patients affected with idiopathic or familial dilated cardiomyopathy. Am J Physiol Heart Circ Physiol 295(3):H1234–H1242
89. Broberg CS, Chugh SS, Conklin C, Sahn DJ, Jerosch-Herold M (2010) Quantification of diffuse myocardial fibrosis and its association with myocardial dysfunction in congenital heart disease. Circ Cardiovasc Imaging 3(6):727–734
90. Goldfarb JW, Zhao W (2014) Magnetic resonance imaging dynamic contrast enhancement (DCE) characteristics of healed myocardial infarction differ from viable myocardium. Magn Reson Imaging 32(10):1191–1197
91. Goldfarb JW, Zhao W (2016) Effects of transcytolemmal water exchange on the assessment of myocardial extracellular volume with cardiovascular MRI. NMR Biomed 29(4):499–506
92. Coelho-Filho OR, Mongeon F-P, Mitchell R, Moreno H, Nadruz W, Kwong R, Jerosch-Herold M (2013) Role of transcytolemmal water-exchange in magnetic resonance measurements of diffuse myocardial fibrosis in hypertensive heart disease. Circ Cardiovasc Imaging 6(1):134–141
93. Treibel TA, Fontana M, Maestrini V, Castelletti S, Rosmini S, Simpson J, Nasis A, Bhuva AN, Bulluck H, Abdel-Gadir A (2016) Automatic measurement of the myocardial interstitium: synthetic extracellular volume quantification without hematocrit sampling. JACC Cardiovasc Imaging 9(1):54–63
94. Fent GJ, Garg P, Foley JRJ, Swoboda PP, Dobson LE, Erhayiem B, Greenwood JP, Plein S, Treibel TA, Moon JC (2017) Synthetic myocardial extracellular volume fraction. JACC Cardiovasc Imaging. doi:10.1016/j.jcmg.2016.12.007
95. Bluemke DA, Kawel-Boehm N (2016) Can a MR imaging scanner accurately measure hematocrit to determine ECV fraction? JACC Cardiovasc Imaging 9(1):64–66
96. Croisille P, De Bourguignon C, Chazot A, Viallon M (2017) Are synthetic haematocrit values derived from blood T1 a good substitute for blood samples to achieve accurate ECV calculation? J Cardiovasc Magn Reson 20(Suppl 1):O28
97. Rauhalammi SM, Mangion K, Barrientos PH, Carrick DJ, Clerfond G, McClure J, McComb C, Radjenovic A, Berry C (2016) Native myocardial longitudinal (T1) relaxation time: regional, age, and sex associations in the healthy adult heart. J Magn Reson Imaging 44(3):541–548
98. Liu C-Y, Liu Y-C, Wu C, Armstrong A, Volpe GJ, Van der Geest RJ, Liu Y, Hundley WG, Gomes AS, Liu S (2013) Evaluation of age-related interstitial myocardial fibrosis with cardiac magnetic resonance contrast-enhanced T1 mapping: MESA (multi-ethnic study of atherosclerosis). J Am Coll Cardiol 62(14):1280–1287
99. Bönner F, Janzarik N, Jacoby C, Spieker M, Schnackenburg B, Range F, Butzbach B, Haberkorn S, Westenfeld R, Neizel-Wittke M (2015) Myocardial T2 mapping reveals age-and sex-related differences in volunteers. J Cardiovasc Magn Reson 17:9
100. Messroghli DR, Plein S, Higgins DM, Walters K, Jones TR, Ridgway JP, Sivananthan MU (2006) Human myocardium: single-breath-hold MR T1 mapping with high spatial resolution—reproducibility study 1. Radiology 238(3):1004–1012
101. Miller CA, Naish JH, Bishop P, Coutts G, Clark D, Zhao S, Ray SG, Yonan N, Williams SG, Flett AS, Moon JC, Greiser A, Parker GJM, Schmitt M (2013) Comprehensive validation of cardiovascular magnetic resonance techniques for the assessment of myocardial extracellular volume. Circ Cardiovasc Imaging 6(3):373–383

102. Atalay MK, Poncelet BP, Kantor HL, Brady TJ, Weisskoff RM (2001) Cardiac susceptibility artifacts arising from the heart-lung interface. Magn Reson Med 45(2):341–345
103. Reeder SB, Faranesh AZ, Boxerman JL, McVeigh ER (1998) In vivo measurement of T* 2 and field inhomogeneity maps in the human heart at 1.5T. Magn Reson Med 39(6):988–998
104. Merlini G, Bellotti V (2003) Molecular mechanisms of amyloidosis. N Engl J Med 349(6):583–596
105. Karamitsos TD, Piechnik SK, Banypersad SM, Fontana M, Ntusi NB, Ferreira VM, Whelan CJ, Myerson SG, Robson MD, Hawkins PN, Neubauer S, Moon JC (2013) Noncontrast T1 mapping for the diagnosis of cardiac amyloidosis. JACC Cardiovasc Imaging 6(4):488–497
106. Maceira AM, Prasad SK, Hawkins PN, Roughton M, Pennell DJ (2008) Cardiovascular magnetic resonance and prognosis in cardiac amyloidosis. J Cardiovasc Magn Reson 10:54
107. Banypersad SM, Fontana M, Maestrini V, Sado DM, Captur G, Petrie A, Piechnik SK, Whelan CJ, Herrey AS, Gillmore JD (2015) T1 mapping and survival in systemic light-chain amyloidosis. Eur Heart J 36(4):244–251
108. O'Mahony C, Elliott P (2010) Anderson-Fabry disease and the heart. Prog Cardiovasc Dis 52(4):326–335
109. Sado DM, White SK, Piechnik SK, Banypersad SM, Treibel T, Captur G, Fontana M, Maestrini V, Flett AS, Robson MD, Lachmann RH, Murphy E, Mehta A, Hughes D, Neubauer S, Elliott PM, Moon JC (2013) Identification and assessment of Anderson-Fabry disease by cardiovascular magnetic resonance noncontrast myocardial T1 mapping. Circ Cardiovasc Imaging 6(3):392–398
110. Thompson RB, Chow K, Khan A, Chan A, Shanks M, Paterson I, Oudit GY (2013) T1 mapping with cardiovascular MRI is highly sensitive for Fabry disease independent of hypertrophy and sex. Circ Cardiovasc Imaging 6(5):637–645
111. Pica S, Sado DM, Maestrini V, Fontana M, White SK, Treibel T, Captur G, Anderson S, Piechnik SK, Robson MD (2014) Reproducibility of native myocardial T1 mapping in the assessment of Fabry disease and its role in early detection of cardiac involvement by cardiovascular magnetic resonance. J Cardiovasc Magn Reson 16:99
112. Hinojar R, Foote L, Ucar EA, Jackson T, Jabbour A, Yu C-Y, McCrohon J, Higgins DM, Carr-White G, Mayr M (2015) Native T1 in discrimination of acute and convalescent stages in patients with clinical diagnosis of myocarditis: a proposed diagnostic algorithm using CMR. JACC Cardiovasc Imaging 8(1):37–46
113. Ferreira VM, Piechnik SK, Dall'Armellina E, Karamitsos TD, Francis JM, Choudhury RP, Friedrich MG, Robson MD, Neubauer S (2012) Non-contrast T1-mapping detects acute myocardial edema with high diagnostic accuracy: a comparison to T2-weighted cardiovascular magnetic resonance. J Cardiovasc Magn Reson 14:42
114. Dawson DK, Neil CJ, Henning A, Cameron D, Jagpal B, Bruce M, Horowitz J, Frenneaux MP (2015) Tako-tsubo cardiomyopathy: a heart stressed out of energy? JACC Cardiovasc Imaging 8(8):985–987
115. Ferreira VM, Piechnik SK, Dall'Armellina E, Karamitsos TD, Francis JM, Ntusi N, Holloway C, Choudhury RP, Kardos A, Robson MD (2013) T1 mapping for the diagnosis of acute myocarditis using CMR: comparison to T2-weighted and late gadolinium enhanced imaging. JACC Cardiovasc Imaging 6(10):1048–1058
116. Dall'Armellina E, Piechnik SK, Ferreira VM, Le Si Q, Robson MD, Francis JM, Cuculi F, Kharbanda RK, Banning AP, Choudhury RP (2012) Cardiovascular magnetic resonance by non contrast T1-mapping allows assessment of severity of injury in acute myocardial infarction. J Cardiovasc Magn Reson 14:15
117. Cameron D, Siddiqi N, Neil CJ, Jagpal B, Bruce M, Higgins DM, He J, Singh S, Redpath TW, Frenneaux MP (2016) T1 mapping for assessment of myocardial injury and microvascular obstruction at one week post myocardial infarction. Eur J Radiol 85(1):279–285
118. O h-Ici D, Jeuthe S, Al-Wakeel N, Berger F, Kuehne T, Kozerke S, Messroghli DR (2014) T1 mapping in ischaemic heart disease. Eur Heart J Cardiovasc Imaging 15(6):597–602
119. Kloner RA, Ganote CE, Jennings RB (1974) The "no-reflow" phenomenon after temporary coronary occlusion in the dog. J Clin Invest 54(6):1496
120. Asanuma T, Tanabe K, Ochiai K, Yoshitomi H, Nakamura K, Murakami Y, Sano K, Shimada T, Murakami R, Morioka S (1997) Relationship between progressive microvascular damage and intramyocardial hemorrhage in patients with reperfused anterior myocardial infarction. Circulation 96(2):448–453
121. Anzalone N, Scotti R, Riva R (2004) Neuroradiologic differential diagnosis of cerebral intraparenchymal hemorrhage. Neurol Sci 25:s3–s5
122. Bulluck H, Rosmini S, Abdel-Gadir A, Bhuva AN, Treibel TA, Fontana M, Gonzalez-Lopez E, Ramlall M, Hamarneh A, Sirker A, Herrey AS, Manisty C, Yellon DM, Moon JC, Hausenloy DJ (2017) Diagnostic performance of T1 and T2 mapping to detect intramyocardial hemorrhage in reperfused ST-segment elevation myocardial infarction (STEMI) patients. J Magn Reson Imaging. doi:10.1002/jmri.25638
123. Mordi I, Radjenovic A, Stanton T, Gardner RS, McPhaden A, Carrick D, Berry C, Tzemos N (2015) Prevalence and prognostic significance of lipomatous metaplasia in patients with prior myocardial infarction. JACC Cardiovasc Imaging 8(9):1111–1112
124. Rakow-Penner R, Daniel B, Yu H, Sawyer-Glover A, Glover GH (2006) Relaxation times of breast tissue at 1.5 T and 3T measured using IDEAL. J Magn Reson Imaging 23(1):87–91
125. Aquaro GD, Todiere G, Strata E, Barison A, Bella G, Lombardi M (2014) Usefulness of india ink artifact in steady-state free precession pulse sequences for detection and quantification of intramyocardial fat. J Magn Reson Imaging 40(1):126–132
126. Mozes FE, Tunnicliffe EM, Pavlides M, Robson MD (2016) Influence of fat on liver T1 measurements using modified Look–Locker inversion recovery (MOLLI) methods at 3T. J Magn Reson Imaging 44(1):105–111
127. Kellman P, Hernando D, Shah S, Zuehlsdorff S, Jerecic R, Mancini C, Liang Z-P, Arai AE (2009) Multiecho dixon fat and water separation method for detecting fibrofatty infiltration in the myocardium. Magn Reson Med 61(1):215–221
128. Larmour S, Chow K, Kellman P, Thompson RB (2016) Characterization of T1 bias in skeletal muscle from fat in MOLLI and SASHA pulse sequences: quantitative fat-fraction imaging with T1 mapping. Magn Reson Med 77(1):237–249
129. Treibel TA, Zemrak F, Sado DM, Banypersad SM, White SK, Maestrini V, Barison A, Patel V, Herrey AS, Davies C (2015) Extracellular volume quantification in isolated hypertension-changes at the detectable limits? J Cardiovasc Magn Reson 17:74
130. Wong TC, Piehler KM, Kang IA, Kadakkal A, Kellman P, Schwartzman DS, Mulukutla SR, Simon MA, Shroff SG, Kuller LH (2013) Myocardial extracellular volume fraction quantified by cardiovascular magnetic resonance is increased in diabetes and associated with mortality and incident heart failure admission. Eur Heart J 35(10):657–664
131. Bernaba BN, Chan JB, Lai CK, Fishbein MC (2010) Pathology of late-onset anthracycline cardiomyopathy. Cardiovasc Pathol 19(5):308–311
132. Neilan TG, Coelho-Filho OR, Shah RV, Feng JH, Pena-Herrera D, Mandry D, Pierre-Mongeon F, Heydari B, Francis SA,

Moslehi J, Kwong RY, Jerosch-Herold M (2013) Myocardial extracellular volume by cardiac magnetic resonance imaging in patients treated with anthracycline-based chemotherapy. Am J Cardiol 111(5):717–722
133. Schelbert EB, Piehler KM, Zareba KM, Moon JC, Ugander M, Messroghli DR, Valeti US, Chang CCH, Shroff SG, Diez J, Miller CA, Schmitt M, Kellman P, Butler J, Gheorghiade M, Wong TC (2015) Myocardial fibrosis quantified by extracellular volume is associated with subsequent hospitalization for heart failure, death, or both across the spectrum of ejection fraction and heart failure stage. J Am Heart Assoc 4(12):e002613
134. Puntmann V (2016) T1-mapping and outcome in nonischemic cardiomyopathy: all-cause mortality and heart failure. JACC Cardiovasc Imaging 9(1):40–50
135. Wong TC, Schelbert EB (2016) Many paths lead to CV outcomes. JACC Cardiovasc Imaging 9(1):24–26
136. Weber KT, Sun Y, Bhattacharya SK, Ahokas RA, Gerling IC (2013) Myofibroblast-mediated mechanisms of pathological remodelling of the heart. Nat Rev Cardiol 10(1):15–26
137. Wong TC, Piehler K, Meier CG, Testa SM, Klock AM, Aneizi AA, Shakesprere J, Kellman P, Shroff SG, Schwartzman DS (2012) Association between extracellular matrix expansion quantified by cardiovascular magnetic resonance and short term mortality. Circulation 126(10):1206–1216
138. Shao J, Liu D, Sung K, Nguyen K-L, Hu P (2016) Accuracy, precision, and reproducibility of myocardial T1 mapping: a comparison of four T1 estimation algorithms for modified Look–Locker inversion recovery (MOLLI). Magn Reson Med. doi:10.1002/mrm.26565
139. Xanthis CG, Bidhult S, Kantasis G, Heiberg E, Arheden H, Aletras AH (2015) Parallel simulations for QUAntifying RElaxation magnetic resonance constants (SQUAREMR): an example towards accurate MOLLI T1 measurements. J Cardiovasc Magn Reson 17:104
140. Sussman MS, Yang IY, Fok KH, Wintersperger BJ (2016) Inversion group (IG) fitting: a new T1 mapping method for modified Look–Locker inversion recovery (MOLLI) that allows arbitrary inversion groupings and rest periods (including no rest period). Magn Reson Med 75(6):2332–2340
141. Blume U, Lockie T, Stehning C, Sinclair S, Uribe S, Razavi R, Schaeffter T (2009) Interleaved T1 and T2 relaxation time mapping for cardiac applications. J Magn Reson Imaging 29(2):480–487
142. Kvernby S, Warntjes MJB, Haraldsson H, Carlhäll C-J, Engvall J, Ebbers T (2014) Simultaneous three-dimensional myocardial T1 and T2 mapping in one breath hold with 3D-QALAS. J Cardiovasc Magn Reson 16(1):102
143. Santini F, Kawel-Boehm N, Greiser A, Bremerich J, Bieri O (2015) Simultaneous T1 and T2 quantification of the myocardium using cardiac balanced-SSFP inversion recovery with interleaved sampling acquisition (CABIRIA). Magn Reson Med 74(2):365–371
144. Akçakaya M, Weingärtner S, Basha TA, Roujol S, Bellm S, Nezafat R (2016) Joint myocardial T1 and T2 mapping using a combination of saturation recovery and T2-preparation. Magn Reson Med 76(3):888–896
145. Ma D, Gulani V, Seiberlich N, Liu K, Sunshine JL, Duerk JL, Griswold MA (2013) Magnetic resonance fingerprinting. Nature 495(7440):187–192
146. Hamilton JI, Jiang Y, Chen Y, Ma D, Lo WC, Griswold M, Seiberlich N (2017) MR fingerprinting for rapid quantification of myocardial T1, T2, and proton spin density. Magn Reson Med 77(4):1446–1458
147. Puntmann VO, Peker E, Chandrashekhar Y, Nagel E (2016) T1 mapping in characterizing myocardial disease. Circ Res 119(2):277–299
148. Captur G, Gatehouse P, Keenan KE, Heslinga FG, Bruehl R, Prothmann M, Graves MJ, Eames RJ, Torlasco C, Benedetti G (2016) A medical device-grade T1 and ECV phantom for global T1 mapping quality assurance—the T1 mapping and ECV standardization in cardiovascular magnetic resonance (T1MES) program. J Cardiovasc Magn Reson 18:58